Hydrothermal and thermal stability of the flame hydrolytic synthesized TiO_2/SiO_2 nano-sized composites

by

Semih Afyon

A Thesis Submitted to the
Graduate School of Engineering
in Partial Fulfillment of the Requirements for
the Degree of

Master of Science
in
Material Science and Engineering
Koc University
July 2009

Koc University

Graduate School of Sciences and Engineering

This is to certify that I have examined this copy of a master's thesis by

Semih Afyon

and have found that it is complete and satisfactory in all respects,
and that any and all revisions required by the final
examining committee have been made.

Committee Members:

_____

Mehmet Somer, Ph. D. (Advisor)

_____

Levent Demirel, Ph. D.

_____

Uğur Ünal, Ph. D.

Date: _____

ABSTRACT

The phase stability of the flame hydrolytic synthesized TiO_2/SiO_2 nano-sized composites has been investigated under thermal and hydrothermal conditions. The pure titania (P25 Evonik Degussa) annealed under hydrothermal conditions (100 g/m^3 absolute humidity, 600 ^oC) was found to have 85 % rutile fraction which was only 46 % when annealed at 600 ^oC without the introduction of humidity. The difference was attributed to the formation of oxygen vacancies under hydrothermal conditions possibly increasing the rate of transformation from anatase to rutile TiO_2. Even the smallest amount of SiO_2 doping was observed to retard the phase transformation and maintain the specific surface area after both thermal and hydrothermal treatments. The highest complete phase transformation temperature (1200 ^oC) and the maximum BET surface area at 1000 ^oC (57 m^2/g) under H_2O atmosphere, were both detected for 24.84 % silica content among TiO_2/SiO_2 composite series. The results obtained from different characterization methods; X-ray powder diffraction, Raman spectroscopy and BET surface area analysis are in good agreement with each other and support the discussed effects of H_2O atmosphere and SiO_2 doping.

ÖZET

Alev hidrolizi yöntemiyle sentezlenmiş, nano boyuttaki TiO_2/SiO_2 kompozitlerinin termal ve hidrotermal kararlılıkları incelenmiştir. Hidrotermal şartlar altında (600 ^oC sıcaklık ve 100 g/m^3 giriş mutlak nemi) işleme tabi tutulmuş saf titanyum dioksit (P25 Evonik Degussa) maddesinin yüzde 85'i rutil fazından oluşurken, bu değer nem verilmeden 600 derecede ısıtılan maddede yüzde 46 olmuştur. Farkın nedeni hidrotermal şartlar altında oluşan oksijen boşluklarına ve bu boşlukların muhtemelen anataz fazından rutil fazına geçişi hızlandırmış olmasına bağlanmıştır. Düşük miktarlarda SiO_2 katkılanan titanyum dioksit kompozitlerinde dahi faz değişim sıcaklığı ile termal ve hidrotermal uygulamalardan sonra korunan spesifik yüzey alanı artmıştır. En yüksek faz değişim sıcaklığı olan 1200 santigrat derece ve 1000 santigrat derece nemli atmosferde korunan maksimum BET yüzey alanı olan 57 m^2/g, % 24.84 silika katkısı olan TiO_2/SiO_2 kompoziti için gözlemlenmiştir. X-ray toz kırınımı, Raman spektroskopi ve BET yüzey alanı analizi gibi değişik karakterizasyon metotlarından elde edilen sonuçlar birbiriyle uyum göstermekte; nemli atmosferin ve SiO_2 katkılamasının tartışılan etkilerini doğrulamaktadır.

ACKNOWLEDGEMENTS

First and foremost, I would like to thank Prof. Dr. Mehmet Somer for giving me the opportunity to work under his guidance in various research projects through my undergraduate and graduate years at Koc University. I am indebted to him for his absolute support and many life lessons he taught to us. I feel very lucky and distinguished by being one of his students.

I also want to thank Dr. Reinhard Vormberg, who is the co-creator of the project that has extended into my master thesis, for his trust at the beginning and guidance through the project.

I would like to extend my gratitude towards Dr. Martin Reisinger for BET measurements, and Prof. Dr. Levent Demirel and Dr. Frank Menzel for their advices and helpful discussions.

I am also grateful to Muharrem Güler, our glass master, without whom it would be quite impossible to build custom-made setups. For the financial support of the project, I want to thank Evonik Degussa GmbH and Koc University.

Furthermore, my sincere thanks to my friends, Ilkin Kokal, Kamil Kiraz and Sinan Öztürk for their invaluable friendship during last seven years. We shared a lot of unforgettable memories and will continue to do so. I would also like to thank Atilla Aşar, Cevriye Koz and Ahmet Topçu for the nice working atmosphere in Inorganic Laboratory. I am also very happy to have two great friends as I finish my master studies, Ali Baş and Yasin Karadağ, with whom I shared the same house for two years.

Finally and most importantly, I want to thank my parents, sister, aunts and grand parents for their unconditional love and support throughout my whole life.

TABLE OF CONTENTS

LIST OF TABLES

LIST OF FIGURES

NOMENCLATURE

XRF	:	X-ray Flourescence
XRD	:	X-Ray Diffraction
BET	:	Brunauer-Emmett-Teller
SSA	:	Specific Surface Area
Nd:YAG	:	Neodymium doped yttrium aluminum garnet
rpm	:	Rotation per minute
θ	:	Bragg angle
λ	:	Wavelength of incident X-rays
β	:	Full width at the half maximum of (101) anatase peak
RIR	:	Reference Intensity Ratio method
μ	:	Linear attenuation coefficient
γ	:	Absolute scale factor
ρ	:	Density
X_α	:	Fraction of a α-phase
X_β	:	Fraction of a β-phase
$\square$	:	Anion vacancy

Chapter 1

INTRODUCTION

TiO_2 has many applications and widely studied in the fields of catalyst carriers [1, 2], photo-catalysis [1-4], semiconductors [5, 6], pigments, self cleaning coatings [7], anti-bacterial agents [8], electronics [9, 10] and various sensors [11, 12].

Titania has three different phases that are rutile, anatase and brookite. Brookite and anatase are metastable phases and transform into thermodynamically stable phase, rutile at high temperatures varying between 400 and 1300 ^oC [13, 14]. The phase transition temperature depends on the presence of foreign cations and anions that may occur as a result of the synthesis method or be intentionally doped [13]. Anatase is the major product in various synthetic routes, such as sol-gel [15], hydrothermal reaction [16], precipitation [17], and flame spray pyrolysis [18]. Also, it has the highest photo-catalytic activity as a result of having lower electron-hole recombination rates and surface energy, and larger specific surface area compared to rutile [19, 20].

According to Inorganic Crystal Structure Database, rutile and anatase crystallize in the tetragonal space group $P\,4_2/mnm$ (no. 136) and $I\,4_1/amd$ (no. 141), with a = 4.5941(1) Å, c = 2.9589(1) Å, $tP6$ for rutile, and a = 3.7842(13) Å, c = 9.5146(15) Å, $tI12$ for anatase, respectively [21]. The characteristic units of both crystal structures are TiO_6 octahedra that are connected to each other by opposite edges and corners for rutile, and by four different edges in a zigzag fashion for anatase condensing along c-axis in both cases. Figure 1.1 & 1.2 shows the crystal structures drawn by using DIAMOND software [22].

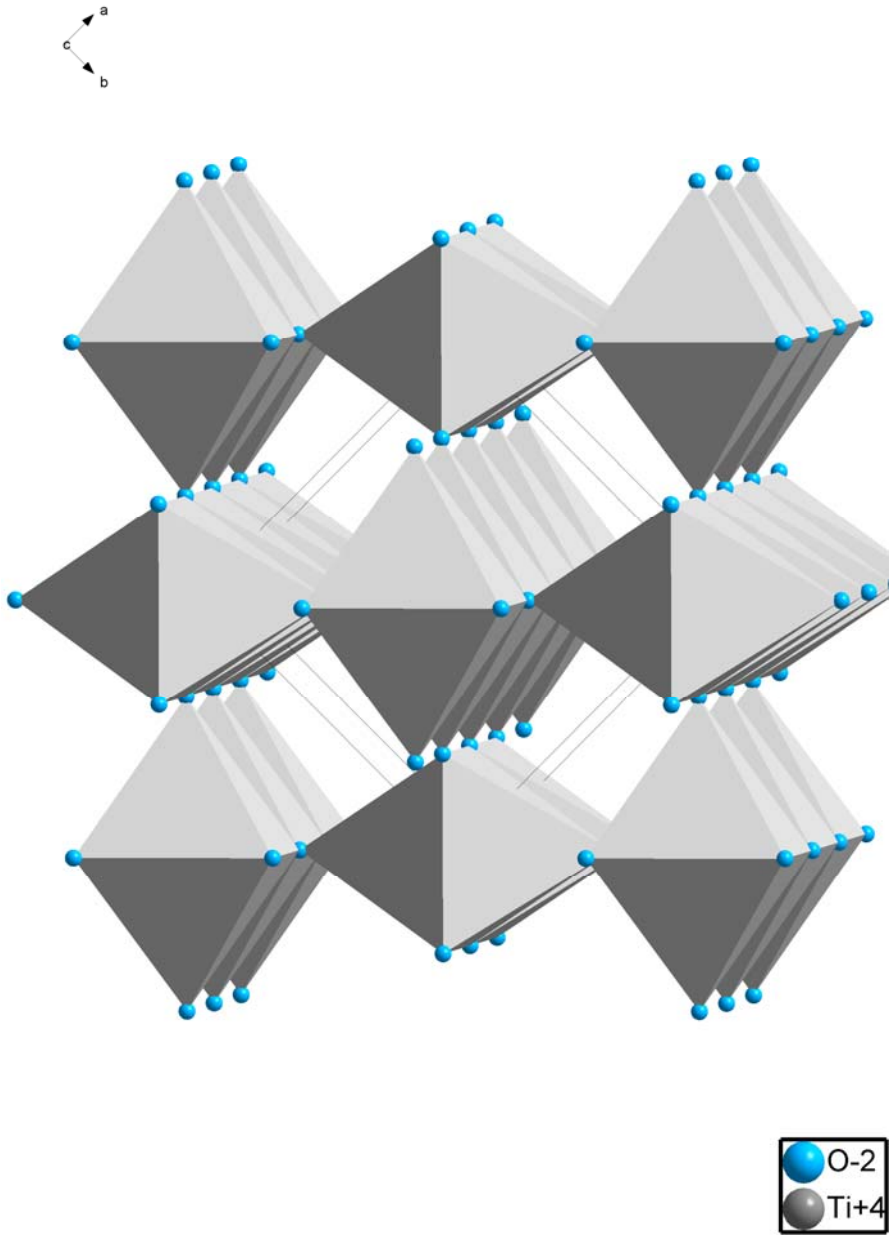

Fig 1.1 The crystal structure of rutile TiO_2.

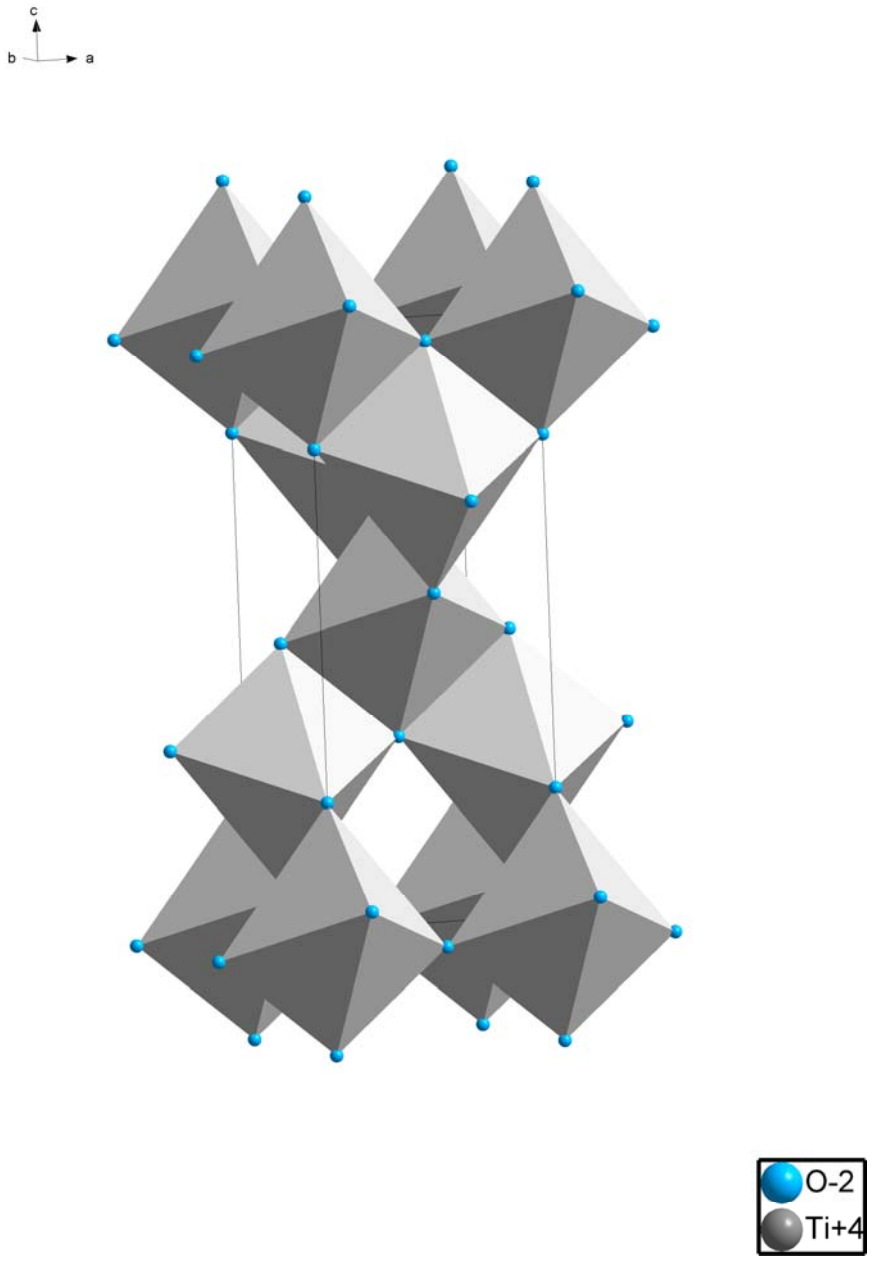

Fig 1.2 The crystal structure of anatase TiO_2.

The aforementioned applications of TiO_2, especially as a catalyst support and photo-catalyst, might require high temperature conditions (600-700 ^oC), where the pure titania would irreversibly transform from anatase to rutile, and had lower activity. Therefore, a considerable amount of research has been done in order to improve the thermal stability of TiO_2, and preserve the anatase phase and specific surface area at high temperatures. The mixed oxide composite systems, such as Al_2O_3/TiO_2, CeO_2/TiO_2, La_2O_3/TiO_2, SnO_2/TiO_2, MoO_3/TiO_2, WO_3/TiO_2, ZrO_2/TiO_2 and SiO_2/TiO_2, synthesized by various methods have been investigated extensively and some gave promising results in terms of thermal stability [2, 14, 18, 23-26]. Among these systems, SiO_2/TiO_2 attracts attention by the phase stability that can go up to 1300 ^oC [14], higher photocatalytic activity and specific surface than undoped titania [4, 25]. In previous studies, SiO_2/TiO_2 composites were usually synthesized by sol-gel method [4, 14, 25], and to our knowledge there were no studies on the flame hydrolytic synthesized TiO_2/SiO_2 composites. Hence, it is important to investigate the TiO_2/SiO_2 nano-sized composites, produced by flame hydrolysis, the AEROSIL® fumed silica process [27]. In this process, the evaporated $TiCl_4$ or $SiCl_4$ is hydrolyzed in an oxyhydrogen flame to produce nano-sized TiO_2 or SiO_2 [28]. The reactions and the synthesis scheme are illustrated in figure 1.3 (from the technical bulletins of Evonik Degussa GmbH). The particle size, the particle size distribution, the specific surface area, and the fraction of different phases could be manipulated by changing the feeding rates of precursors, the concentration of coreactants, the temperature, and the dwell time of materials inside the combustion chamber [1, 28].

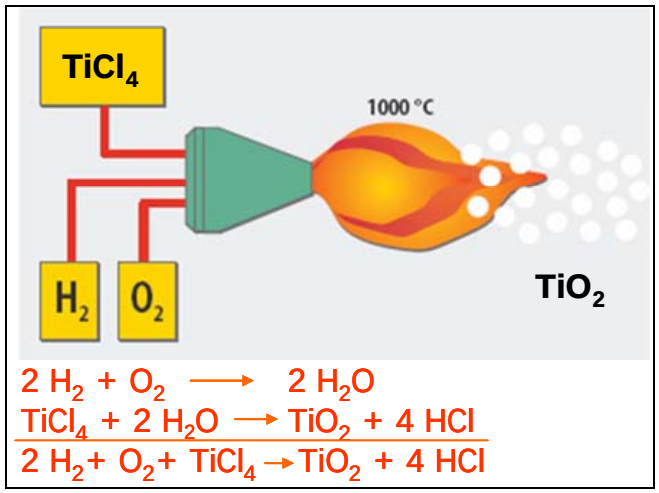

Fig 1.3 Scheme for the synthesis of TiO_2 by flame hydrolysis, AEROSIL® process [28].

Another important challenge for the catalytic uses of TiO_2 could be the working atmosphere; especially in catalytic converters, where water vapor is released by the combustion of hydrocarbons generating harsh hydrothermal conditions that could negatively affect the phase stability and specific surface area of TiO_2. Iida et. al. and Shannon et al. studied the effect of vacuum and H_2 atmospheres in the past and concluded that the rate of transformation from anatase to rutile decreases as the oxygen partial pressure increases, whereas it is elevated by the formation of oxygen vacancies under H_2 and other reducing atmospheres [29, 13]. In more recent studies, same conclusions about the oxygen partial pressure and the effect of reducing atmospheres were drawn again with various atmospheres (Cl_2/Ar, Ar/air) and test techniques [30, 31]. However, there is a lack of research on H_2O atmosphere, which is considered to be essential if TiO_2 is intended to be used in catalytic converters as the catalyst support material.

In this present study, the phase stability of the flame hydrolytic synthesized TiO_2/SiO_2 nano-sized composites under both thermal and hydrothermal conditions, and the influence of SiO_2 content on the specific surface area and the phase stability have been investigated in detail.

Chapter 2

EXPERIMENTAL METHODS

2.1 Introduction

Due to the nano-nature of TiO_2 materials that might be harmful for the respiratory system, all manipulations and experimental preparations were done under the hood with proper safety precautions, such as the usage of protective masks and gloves. Also, the annealing process of samples is needed to be done extremely careful in order to prevent skin burns and fire.

2.2 Materials

TiO_2/SiO_2 nano-sized composite series, produced by flame hydrolysis, the AEROSIL® fumed silica process [27] are the R&D products of Evonik Degussa GmbH. In total, 40 mixed oxide systems were analyzed in this study, and 5 representatives containing 0 % (Evonik Degussa, TiO_2 P 25), 0.54 mol % SiO_2, 4.53 mol % SiO_2, 9.71 mol % SiO_2 and 24.84 mol % SiO_2 are going to be discussed in detail. The silica contents were verified at Analytical Laboratories of Evonik Degussa GmbH by Panalytical Axios XRF Spectrometer equipped with X-ray tube: Rh-anode SST and SuperQ4 software. Both anatase and rutile phases exist in the composite series with varying amounts for different silica contents.

2.3 Sample Preparations:

The Titanium Dioxide P 25 powder has an approximate value of 96 % air content [32], and TiO_2/SiO_2 powders seem to be similar and need to be densified in order to place reasonable amounts of test materials in the crucibles for annealing procedure.

2.3.1 Preparation of the dispersion

Approximately 100g of TiO_2 powder was dispersed in one liter distilled water with Ika Ultra-Turrax DI 25 (Fig.2.1) at 20.000 rpm. In order to prevent the agglomeration, the powder was added slowly in 6-7 minutes and then treated with the ultra-turrax for 15 minutes.

Figure 2.1 Ika Ultra-Turrax DI 25.

2.3.2 Drying

The dispersions were transferred into suitable glass containers and the water content of dispersions was evaporated at 105 ^{o}C for 48 hours (Figure 2.2).

Figure 2.2 Examples of dried dispersions.

2.3.3 Mortaring & Sieving

The dried samples were roughly mortared and sieved for ten minutes at the maximum speed. TiO_2 particles above 38 microns were collected and the residue was disposed. Typically, the residue does not exceed 10 grams for a starting sample of 100 grams.

(a) (b)

(c) (d)

Figure 2.3 (a) Samples before mortaring, (b) Samples after mortaring, (c) Sieving machine, (d) The residue and the collected material after sieving.

2.4 Annealing of granulated TiO_2/SiO_2 powders:

All samples were annealed for four hours at the following temperatures in muffle furnace (Thermal conditions) and in tube furnace (Hydrothermal conditions); 500, 600, 700, 800, 900, 1000, 1100, 1200 ^oC.

2.4.1 Experimental Setup (Thermal Conditions)

The prepared samples were weighed about 2.5 grams and placed in Al_2O_3 crucibles. The crucibles were planted in the muffle furnace (Nabertherm ®), which can be programmed within the temperature range 20-1100 ^oC, and the furnace was heated to the aforementioned temperatures. After annealing four hours at the specific temperature, the crucibles were taken out for cooling. The cooled test samples were labeled as “M series” (Ex: M5 for the test sample annealed in muffle furnace at 500 ^oC).

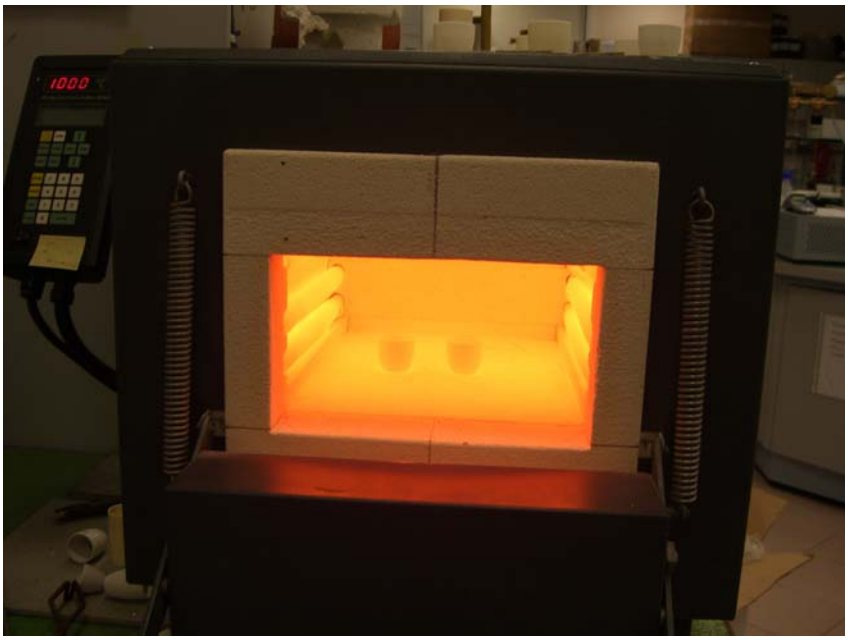

Figure 2.4 Annealing process in the muffle furnace.

2.4.2 Experimental Setup (Hydrothermal Conditions)

The hydrothermal conditions inside the tube furnace were satisfied by a setup, where water vapor was obtained at 50-60^{o}C and then carried to the tube furnace with a flow rate of 6.4 ± 0.2 l/min. The condensation of water vapor before reaching the furnace was prevented by a heating belt around glass tubes, and the humidity values of the gas were monitored just before entering the tube furnace. Figures 2.5 and 2.6 show the experimental setup scheme and the actual design, respectively.

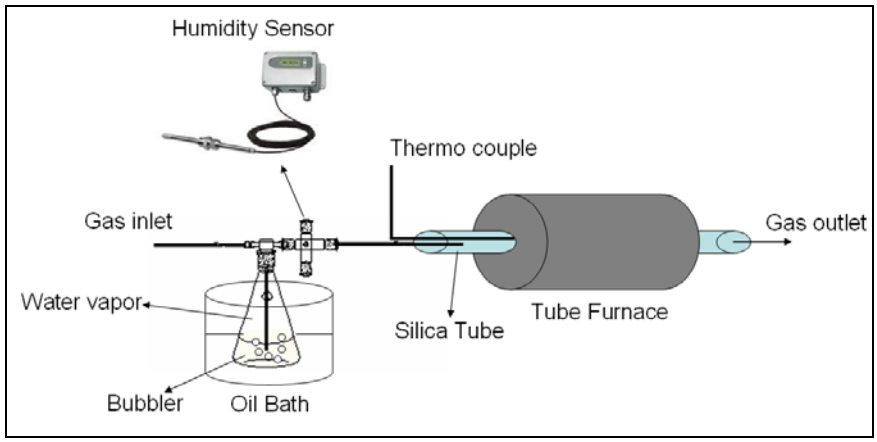

Figure 2.5 The hydrothermal setup scheme.

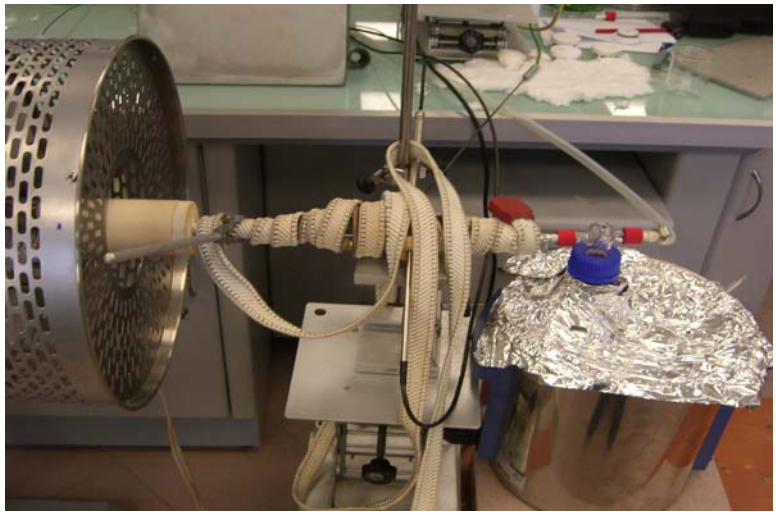

Figure 2.6 The actual design.

Depending on the variations of temperature and pressure, the absolute humidity was adjusted to 100 ± 15 g/m^3. The humidity values were recorded with the E+E Elektronik EE33 data-software [33] by 5 seconds intervals, and Figure 2.7 shows a typical output.

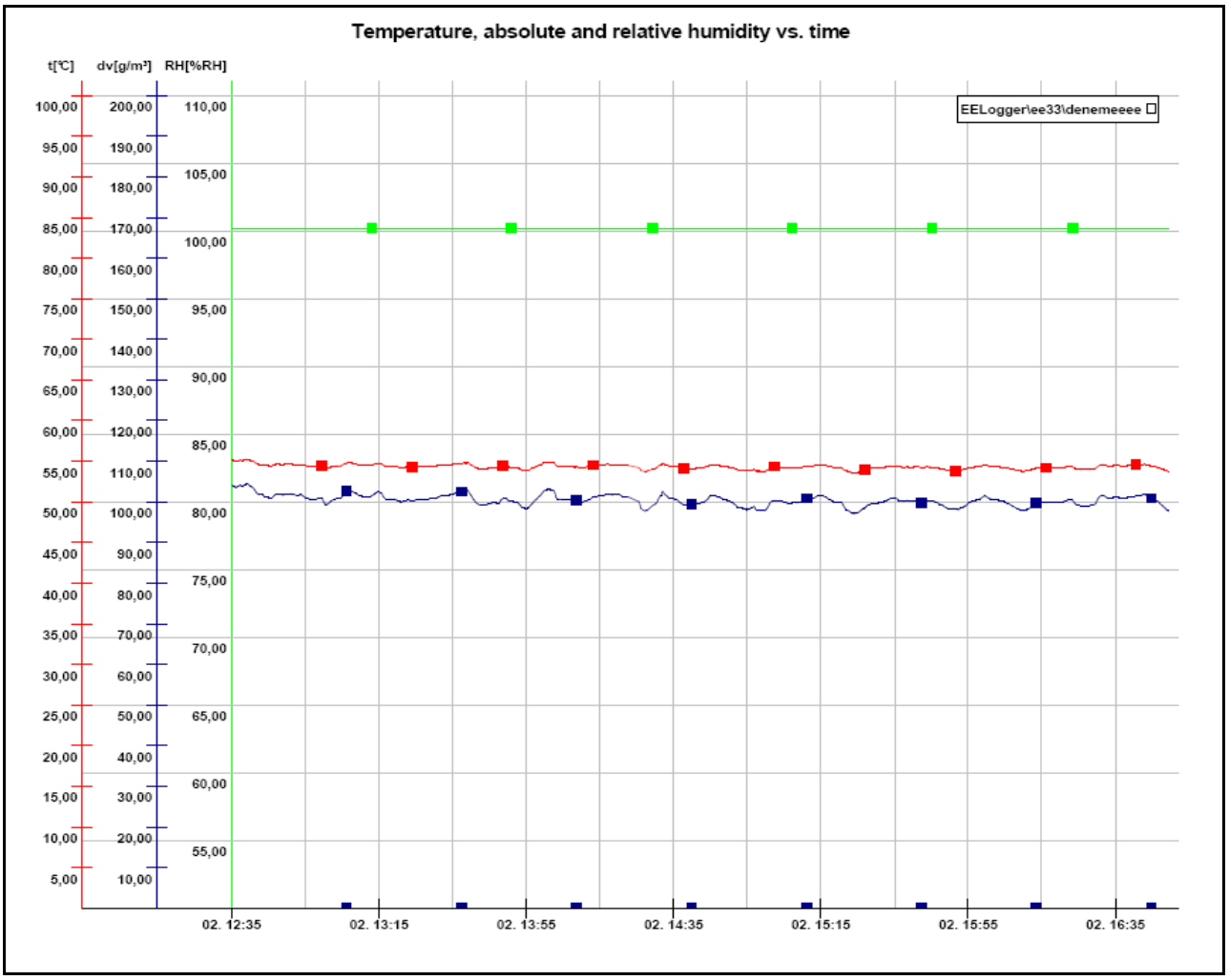

Figure 2.7 The plot of humidity values recorded for four hours.

Similar to M-series the prepared samples were weighed about 2.5 grams and placed in Al_2O_3 combustion boats. The boats on a silica baker's peel were placed in the tube furnace (Protherm ®), which can be programmed within the temperature range 20-1500 ^oC, and the furnace was heated to the aforementioned temperatures. After annealing four hours at the specific temperature under hydrothermal conditions, the boats were taken out for cooling.

The cooled test samples were labeled as “T series” (Ex: T5 for the test sample annealed in tube furnace at 500 ^{o}C under hydrothermal conditions).

Figure 2.8 Annealing process in the tube furnace under hydrothermal conditions.

2.5 Materials Characterization:

2.5.1 X-Ray Powder Diffraction

In order to perform X-ray powder diffraction, the test samples were finely grained and sandwiched between two Mylar® Polyester films by using special aluminum sample holders (Figure 2.9). Thoroughly, the first film was placed on the holder ring and the powder was spread on the film. After coating the periphery of the film with silicon fat to ensure sealing, the second protecting film was planted and tightened on top of the first one with a second aluminum ring.

Figure 2.9 X-ray sample holders.

X-ray powder diffraction patterns of test samples were acquired with an Imaging Plate Huber G670 equipped with a germanium monochromator and $CuK_{\alpha 1}$ radiation (Figure 2.10), and the data was collected in the range $3^o \leq 2\theta \leq 100^o$ with a step size of 0.005° 2θ. For the preliminary analysis, Stoe WinXPOW Software [34] was used to compare experimental XRD patterns with Inorganic Crystal Structure Database (ICSD) [21].

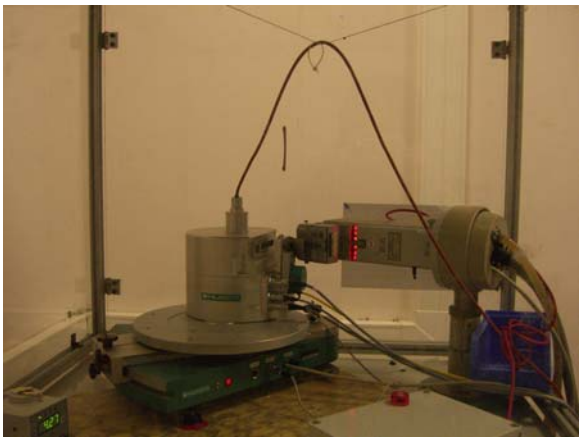

Figure 2.10 X-ray Powder Diffractometer.

The quantitative phase analysis for the test samples were done by using Match! Software [34] based on (101), (004), (200) and (211) peaks of anatase, and (110), (101) and (221) peaks of rutile. The average crystallite sizes of anatase particles in TiO_2/SiO_2 composites were calculated with the Scherrer equation:

$$\text{Crystallite size} = 0.9\lambda / (\beta \cos\theta)$$

where λ is the wavelength of incident X-rays, β is the full width at the half maximum of (101) anatase peak, and θ is the Bragg angle.

2.5.2 Raman Spectroscopy

Raman spectra of annealed and as-prepared samples were obtained with a Bruker RFS 100/S Raman spectrometer (Silica capillary, Ø 4mm) equipped with Nd: YAG-Laser (1064 nm, 200 mW).

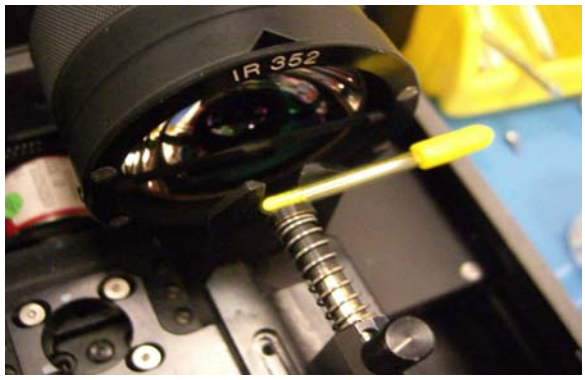

Figure 2.11 TiO_2/SiO_2 test sample positioned in Raman spectrometer.

2.5.3 BET Surface Area

The surface area measurements were done at Analytical Laboratories of Evonik Degussa GmbH by the Brunauer-Emmett-Teller (BET) method with nitrogen adsorption using TriStar 3000 V6.08 A.

Chapter 3

RESULTS & DISCUSSION

3.1 XRD powder diffraction characterization:

Figure 3.1.1 shows the theoretical XRD patterns for anatase and rutile TiO_2. The most intense diffraction peaks of rutile and anatase do not overlap, and the phase transformation can be easily tracked by means of X-ray powder diffraction.

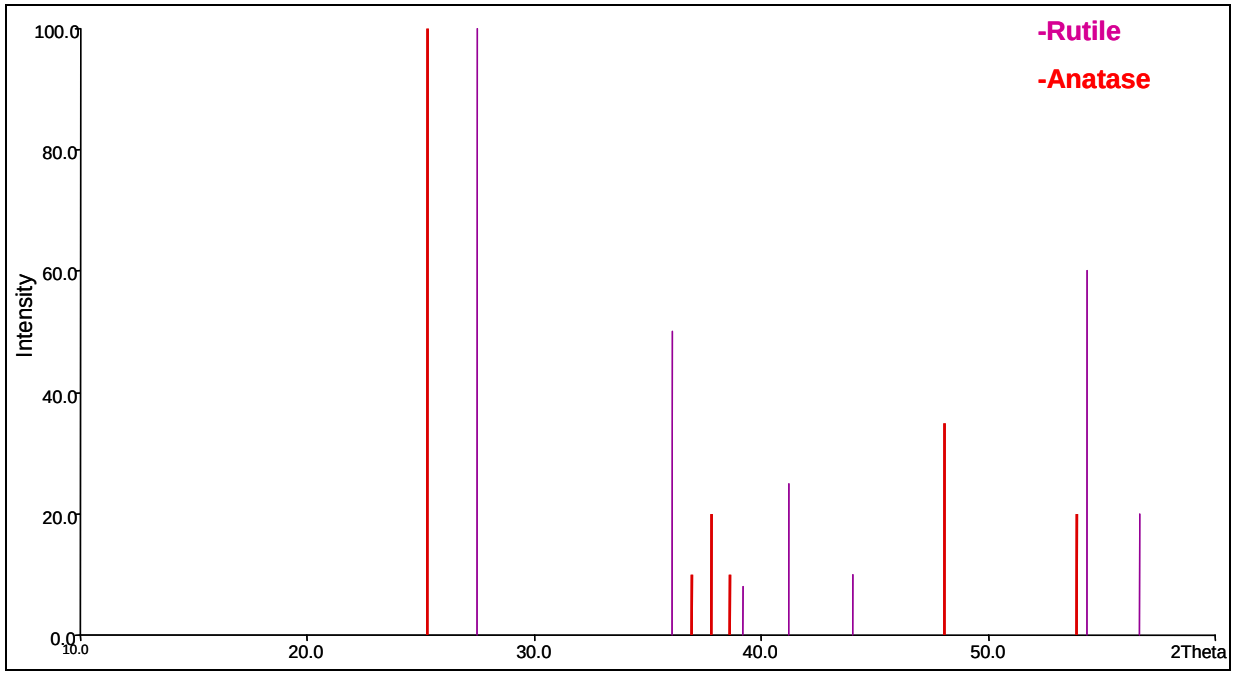

Figure 3.1.1 Theoretical XRD pattern for anatase and rutile [34].

The X-ray Powder patterns of test samples as-prepared and annealed at various critical temperatures, where there have been considerable amount of changes in intensities of rutile TiO_2 diffraction peaks under thermal and hydrothermal conditions are illustrated in Figure 3.1.2 series. The change in intensity of the diffraction peak ($2\theta = 27.447$) mainly confirms the start of phase transformation and the increase in rutile fraction that will be discussed in the further text. The XRD patterns of the test samples annealed at the temperatures other than the critical temperatures shown in Figure 3.1.2 series are illustrated in Appendix A for hydrothermal conditions and in Appendix B for thermal conditions.

No extra diffraction peaks due to another crystalline phase were detected even at 1200 ^oC. This was the case for all TiO_2/SiO_2 nano-sized composite series including the highest SiO_2 content, 24.84 %, which is a good indication of the incorporation of SiO_2 into titania matrix. Even though no crystalline phase of SiO_2 was detected, there is a possibility that SiO_2 might still exist separately as an amorphous phase. This possibility is discussed by means of Raman characterization in section 3.2.

The existence of both anatase and rutile phases with varying amounts for different silica contents could be qualitatively observed by differing intensities of ($2\theta = 27.447$) diffraction peak in as-prepared samples of composite series. The start and completion of phase transformation are directly comparable for M (thermal) and T (hydrothermal) series, but there are differences in terms of rutile and anatase TiO_2 diffraction peak intensities at the critical temperatures. The difference is maximum for undoped titania and diminished with SiO_2 doping. The smaller particle sizes for SiO_2 doped TiO_2 compared to undoped titania is also crudely observable by the broader diffraction peaks of these samples. These qualitative observations for phase analysis and particle size are confirmed by quantitative methods.

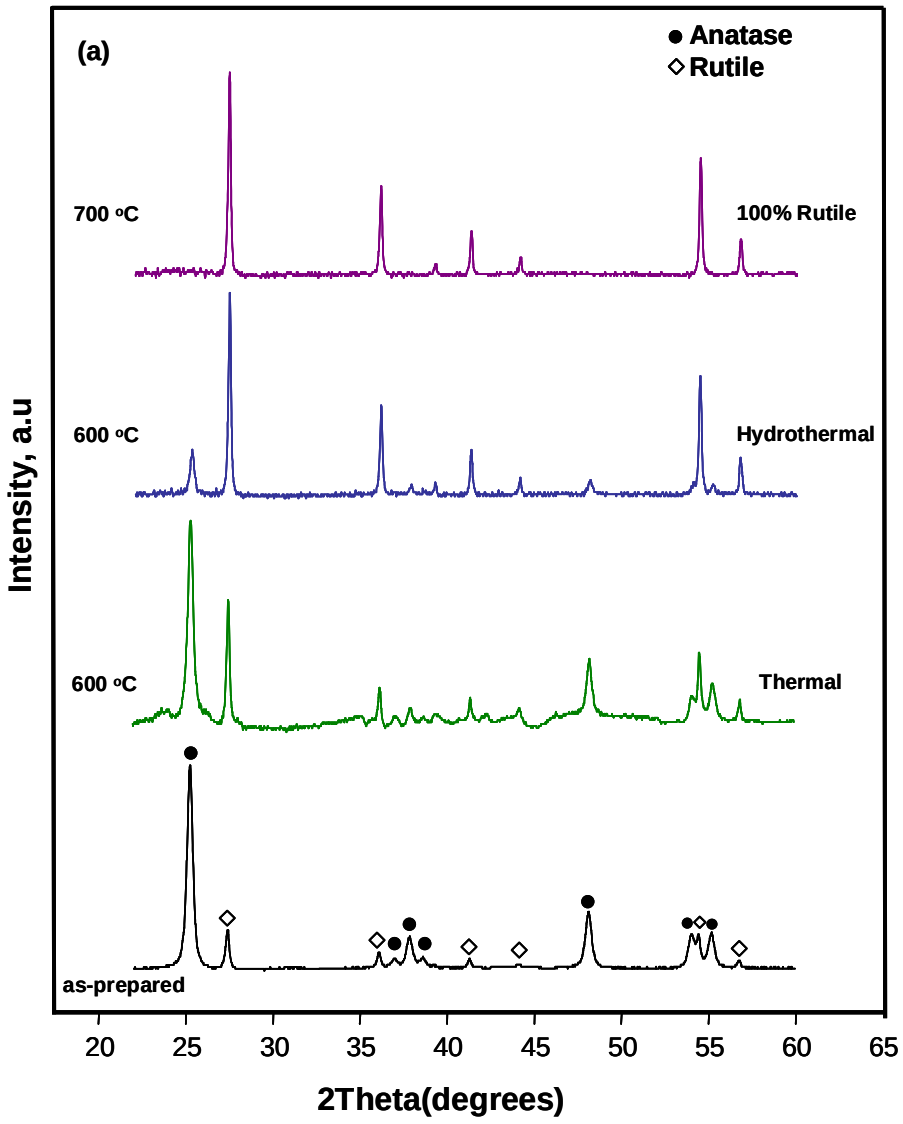

Figure 3.1.2.a XRD patterns of TiO_2 with 0 % silica content, as-prepared and at phase transformation temperatures under thermal and hydrothermal conditions.

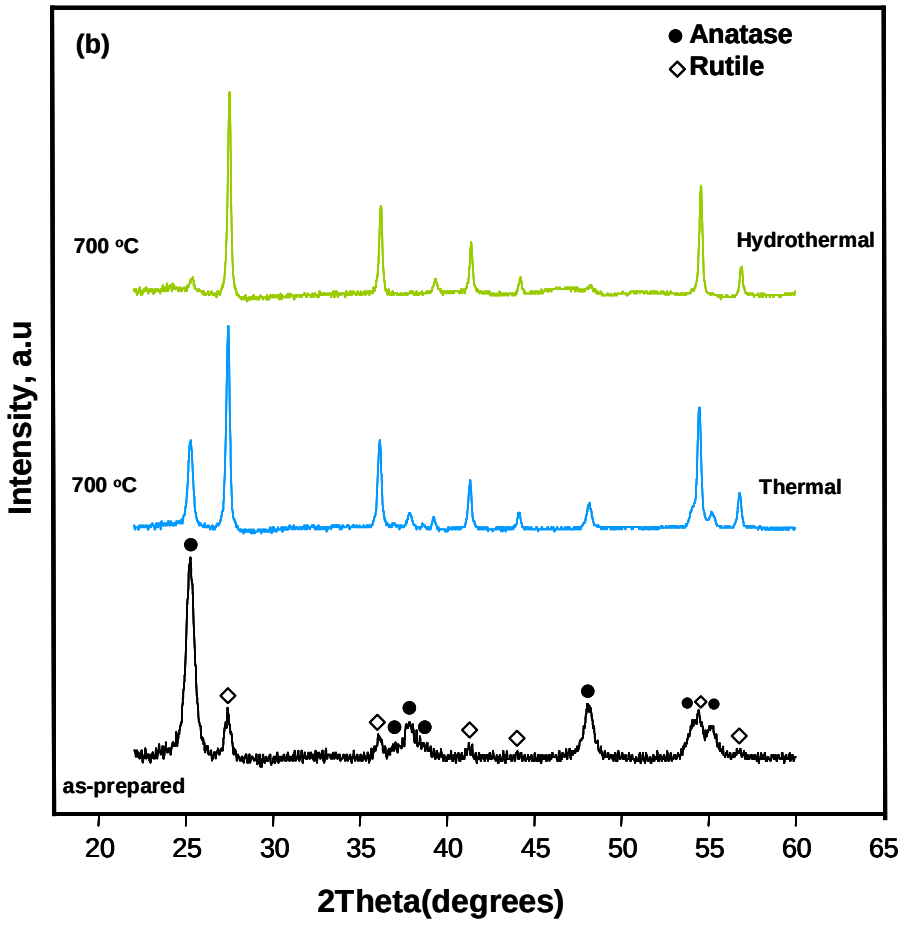

Figure 3.1.2.b XRD patterns of TiO_2 with 0.54 % silica content, as-prepared and at phase transformation temperatures under thermal and hydrothermal conditions.

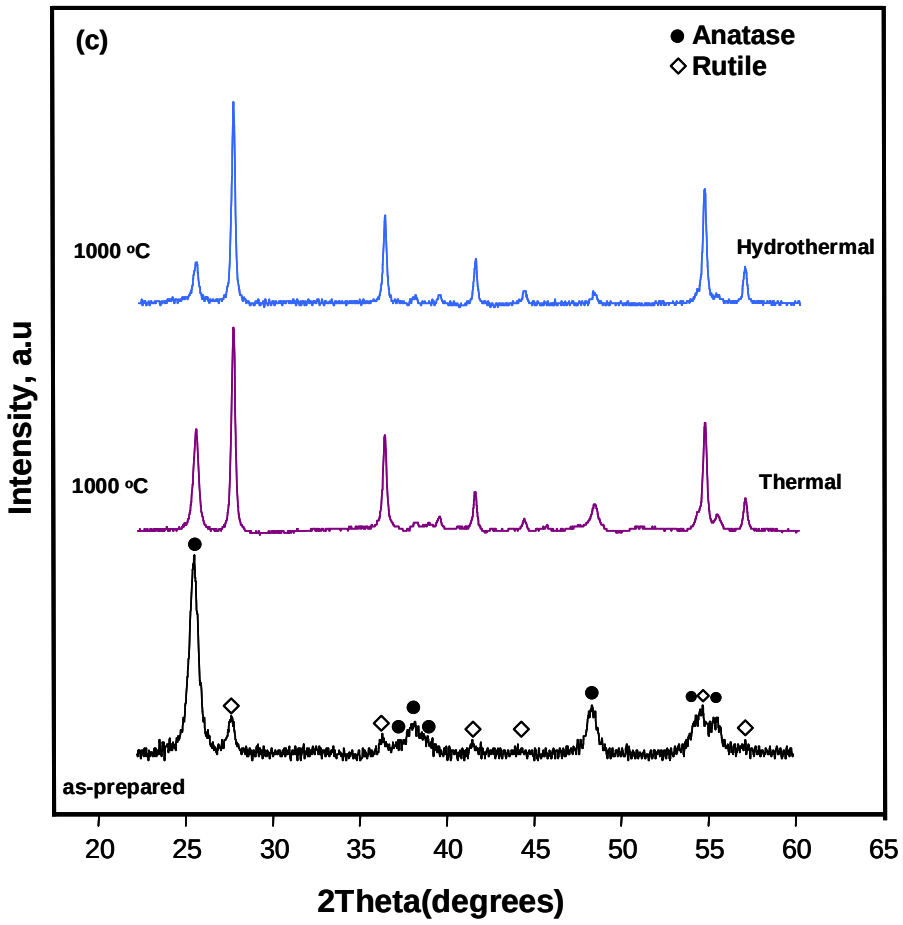

Figure 3.1.2.c XRD patterns of TiO_2 with 4.53 % silica content, as-prepared and at phase transformation temperatures under thermal and hydrothermal conditions.

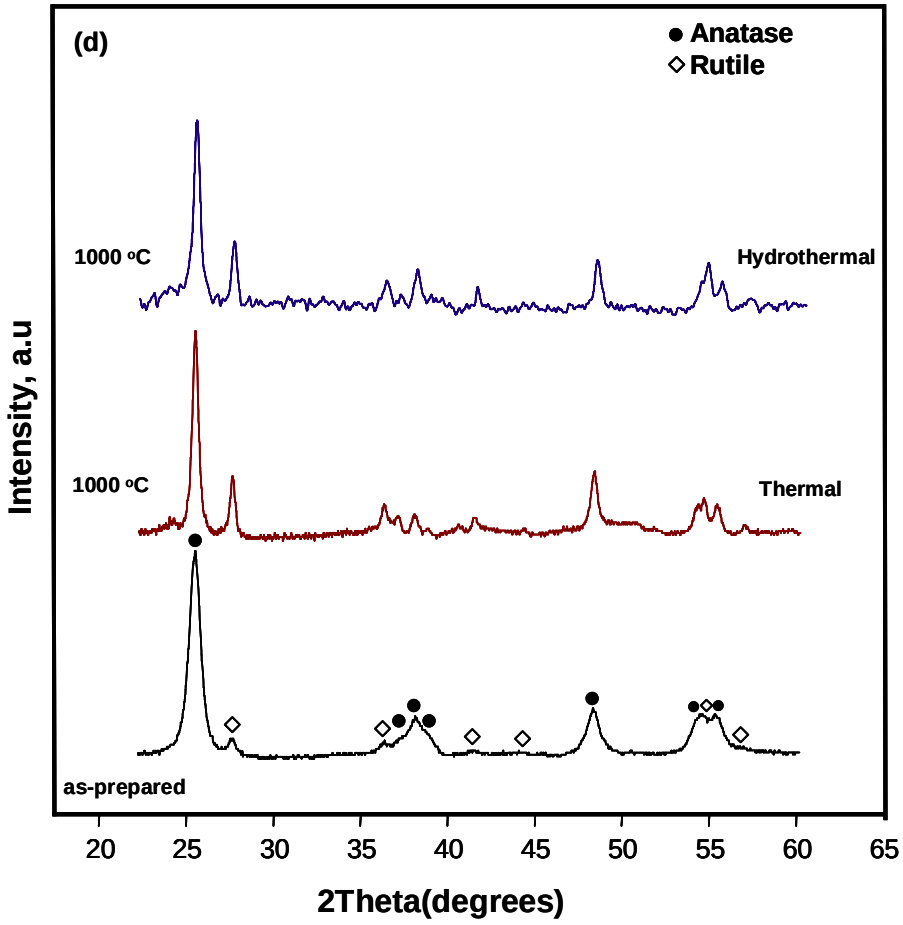

Figure 3.1.2.d XRD patterns of TiO_2 with 9.71 % silica content, as-prepared and at phase transformation temperatures under thermal and hydrothermal conditions.

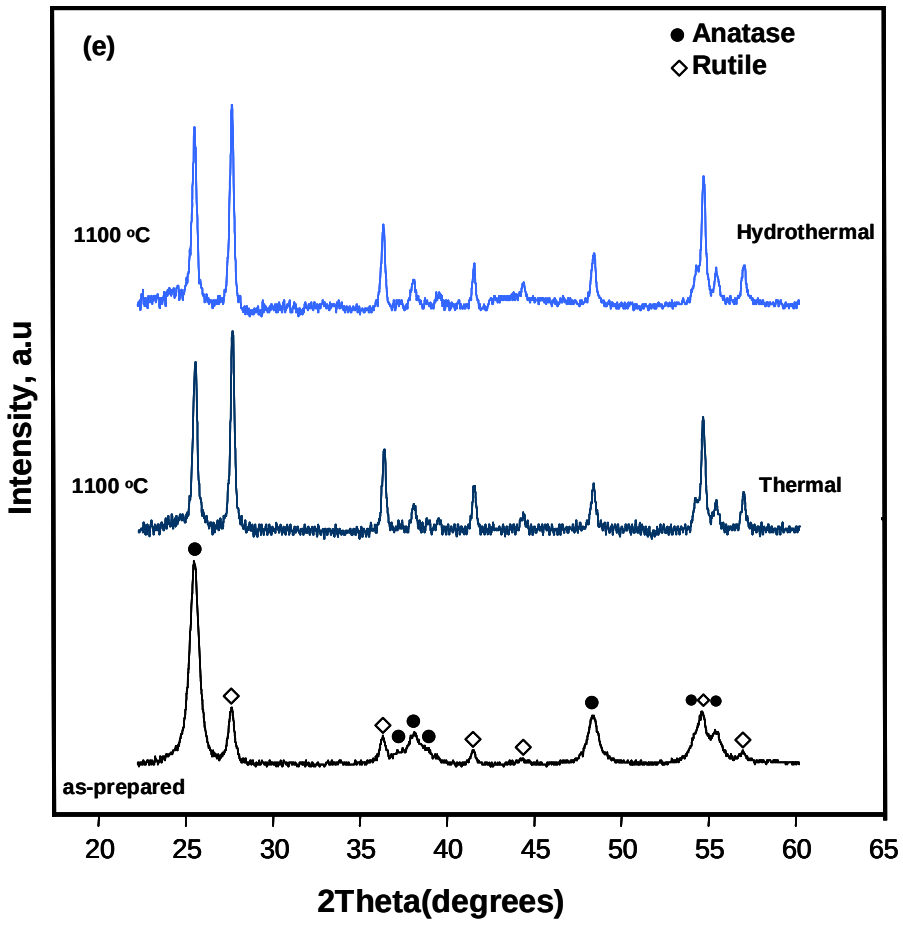

Figure 3.1.2.e XRD patterns of TiO_2 with 24.84 % silica content, as-prepared and at phase transformation temperatures under thermal and hydrothermal conditions.

The quantitative phase analysis for the test samples was performed by using Match! Software that applies "Reference Intensity Ratio method" (RiR-method) for the calculation [35].

The concentration of analyte is one of the factors that affect the intensity of a diffraction peak; the RIR method scales all diffraction data to a standard reference, corundum (α-Al_2O_3), and the factors other than the analyte concentration are reduced to a constant [36]. The scale factor, (Intensity Analyte / Intensity Corundum = I/Ic), can be determined experimentally by obtaining the ratio of diffraction peaks in a 50/50 weight mixture of analyte and the corundum. It can also be calculated according to below equation if the crystal structure is known:

$$I/Ic = \mu \gamma \rho c / \mu c \gamma c \rho$$

where μ is the linear attenuation coefficient, γ is the absolute scale factor, and ρ is the density [36]. As the scale factors are known, the weight fractions of phases, X_α and X_β, in a $\alpha+\beta$ mixture can be calculated with the following equation:

$$(I/Ic)_\alpha / (I/Ic)_\beta = X_\alpha / X_\beta$$

Table 3.1.1 series show the phase analysis results for hydrothermal treated samples with 0, 0.54, 4.53, 9.71, 24.84 % silica contents. The calculations for “two peaks results” are carried out by using only the most intense peaks (2θ = 25.281, (101) for anatase), and (2θ = 27.447, (110) for rutile), “all peaks results” are done for the peaks (2θ = 25,281, 37.801, 48.050, 55.062 for anatase) and (2θ = 27.447, 36.086, 54.323 for rutile). It is expected that there might be an error of plus or minus 3 % for the phase analysis depending on the quality of the X-ray powder data, and this value might go up to 5% for low crystalline samples.

Table 3.1.1.a The phase analysis results of titania with 0 % silica content (T-series).

0 % SiO_2		all peaks	all peaks	two peaks	two peaks
Lot Nr.	Temperature °C	Rutile [%]	Anatase [%]	Rutile [%]	Anatase [%]
502260-A	0	22.70	77.30	21.20	78.80
502260-T5	500	32.40	67.60	30.70	69.30
502260-T6	600	85.40	14.60	85.60	14.40
502260-T7	700	100.00	0.00	100.00	0.00
502260-T8	800	100.00	0.00	100.00	0.00
502260-T9	900	100.00	0.00	100.00	0.00
502260-T10	1000	100.00	0.00	100.00	0.00
502260-T11	1100	100.00	0.00	100.00	0.00
502260-T12	1200	100.00	0.00	100.00	0.00

Table 3.1.1.b The phase analysis results of titania with 0.54 % silica content (T-series).

0.54 % SiO_2		all peaks	all peaks	two peaks	two peaks
Lot Nr.	Temperature °C	Rutile [%]	Anatase [%]	Rutile [%]	Anatase [%]
4305-A	0	29.30	70.70	26.90	73.10
4305-T5	500	30.40	69.60	27.70	72.30
4305-T6	600	45.10	54.90	42.20	57.80
4305-T7	700	94.00	6.00	94.30	5.70
4305-T8	800	100.00	0.00	100.00	0.00
4305-T9	900	100.00	0.00	100.00	0.00
4305-T10	1000	100.00	0.00	100.00	0.00
4305-T11	1100	100.00	0.00	100.00	0.00
4305-T12	1200	100.00	0.00	100.00	0.00

Table 3.1.1.c The phase analysis results of titania with 4.53 % silica content (T-series).

4.53 % SiO_2		all peaks	all peaks	two peaks	two peaks
Lot Nr.	Temperature °C	Rutile [%]	Anatase [%]	Rutile [%]	Anatase [%]
4304-A	0	27.30	72.70	22.80	77.20
4304-T5	500	25.10	74.90	22.20	77.80
4304-T6	600	26.20	73.80	21.90	78.10
4304-T7	700	27.90	72.10	26.30	73.70
4304-T8	800	24.40	75.60	21.80	78.20
4304-T9	900	31.70	68.30	27.10	72.90
4304-T10	1000	88.00	12.00	88.00	12.00
4304-T11	1100	100.00	0.00	100.00	0.00
4304-T12	1200	100.00	0.00	100.00	0.00

Table 3.1.1.d The phase analysis results of titania with 9.71 % silica content (T-series).

9.71 % SiO_2 Lot Nr.	Temperature °C	all peaks Rutile [%]	all peaks Anatase [%]	two peaks Rutile [%]	two peaks Anatase [%]
4294-A	0	14.70	85.30	9.50	90.50
4294-T5	500	15.70	84.30	14.70	85.30
4294-T6	600	19.70	80.30	15.50	84.50
4294-T7	700	18.80	81.20	13.50	86.50
4294-T8	800	19.50	80.50	15.70	84.30
4294-T9	900	19.00	81.00	16.00	84.00
4294-T10	1000	37.30	62.70	35.40	64.60
4294-T11	1100	100.00	0.00	100.00	0.00
4294-T12	1200	100.00	0.00	100.00	0.00

Table 3.1.1.e The phase analysis results of titania with 24.84 % silica content (T-series).

24.84 % SiO_2 Lot Nr.	Temperature °C	all peaks Rutile [%]	all peaks Anatase [%]	two peaks Rutile [%]	two peaks Anatase [%]
4292-A	0	30.80	69.20	27.90	72.10
4292-T5	500	32.80	67.20	30.30	69.70
4292-T6	600	31.50	68.50	28.50	71.50
4292-T7	700	31.70	68.30	28.50	71.50
4292-T8	800	31.60	68.40	28.30	71.70
4292-T9	900	30.70	69.30	27.50	72.50
4292-T10	1000	30.50	69.50	28.40	71.60
4292-T11	1100	62.20	37.80	61.60	38.40
4292-T12	1200	100.00	0.00	100.00	0.00

Table 3.1.2 series show the phase analysis results for thermal treated samples with 0, 0.54, 4.53, 9.71, 24.84 % silica contents. The anatase and rutile fractions are very close to ones that are calculated for hydrothermal series within the experimental error, except in the range where the phase transformation was observed.

Table 3.1.2.a The phase analysis results of titania with 0 % silica content (M-series).

0 % SiO_2 Lot Nr.	Temperature °C	all peaks Rutile [%]	all peaks Anatase [%]	two peaks Rutile [%]	two peaks Anatase [%]
502260-A	0	22.70	77.30	21.20	78.80
502260-M5	500	26.50	73.50	24.50	74.50
502260-M6	600	46.00	54.00	46.70	53.30
502260-M7	700	100.00	0.00	100.00	0.00
502260-M8	800	100.00	0.00	100.00	0.00
502260-M9	900	100.00	0.00	100.00	0.00
502260-M10	1000	100.00	0.00	100.00	0.00
502260-M11	1100	100.00	0.00	100.00	0.00
502260-M12	1200	100.00	0.00	100.00	0.00

Table 3.1.2.b The phase analysis results of titania with 0.54 % silica content (M-series).

0.54 % SiO_2 Lot Nr.	Temperature °C	all peaks Rutile [%]	all peaks Anatase [%]	two peaks Rutile [%]	two peaks Anatase [%]
4305-A	0	29.30	70.70	26.90	73.10
4305-M5	500	33.10	66.90	30.30	69.70
4305-M6	600	41.00	59.00	39.20	60.80
4305-M7	700	64.60	35.40	65.00	35.00
4305-M8	800	100.00	0.00	100.00	0.00
4305-M9	900	100.00	0.00	100.00	0.00
4305-M10	1000	100.00	0.00	100.00	0.00
4305-M11	1100	100.00	0.00	100.00	0.00
4305-M12	1200	100.00	0.00	100.00	0.00

Table 3.1.2.c The phase analysis results of titania with 4.53 % silica content (M-series).

4.53 % SiO_2 Lot Nr.	Temperature °C	all peaks Rutile [%]	all peaks Anatase [%]	two peaks Rutile [%]	two peaks Anatase [%]
4304-A	0	27.30	72.70	22.80	77.20
4304-M5	500	28.00	72.00	26.70	73.30
4304-M6	600	22.30	77.70	19.70	80.30
4304-M7	700	23.80	76.20	20.10	79.90
4304-M8	800	23.40	76.40	21.20	78.80
4304-M9	900	27.40	72.60	28.90	71.10
4304-M10	1000	77.20	22.80	77.20	22.80
4304-M11	1100	100.00	0.00	100.00	0.00
4304-M12	1200	100.00	0.00	100.00	0.00

Table 3.1.2.d The phase analysis results of titania with 9.71 % silica content (M-series).

9.71 % SiO_2		all peaks	all peaks	two peaks	two peaks
Lot Nr.	Temperature °C	Rutile [%]	Anatase [%]	Rutile [%]	Anatase [%]
4294-A	0	14.70	85.30	9.50	90.50
4294-M5	500	15.20	84.80	13.50	86.50
4294-M6	600	14.20	85.80	9.60	90.40
4294-M7	700	18.60	81.40	15.70	84.30
4294-M8	800	18.70	81.30	15.60	84.40
4294-M9	900	14.30	85.70	11.30	88.70
4294-M10	1000	29.50	70.50	29.40	70.60
4294-M11	1100	96.80	3.20	96.90	3.10
4294-M12	1200	100.00	0.00	100.00	0.00

Table 3.1.2.e The phase analysis results of titania with 24.84 % silica content (M-series).

24.84 % SiO_2		all peaks	all peaks	two peaks	two peaks
Lot Nr.	Temperature °C	Rutile [%]	Anatase [%]	Rutile [%]	Anatase [%]
4292-A	0	30.80	69.20	27.90	72.10
4292-M5	500	32.10	67.90	29.60	70.40
4292-M6	600	33.00	67.00	30.40	69.60
4292-M7	700	32.50	67.50	30.00	70.00
4292-M8	800	31.20	68.80	27.60	72.40
4292-M9	900	30.80	69.20	30.20	69.80
4292-M10	1000	30.90	69.10	28.90	71.10
4292-M11	1100	63.20	36.80	63.10	36.90
4292-M12	1200	100.00	0.00	100.00	0.00

It has been commonly reported that the dopant addition into titania matrix can effectively inhibit the phase transformation from rutile to anatase via retarding the grain growth [4, 18, 25, 26]. The crystallite size of TiO_2 could be decreased by the accumulation of the dopant cation at the grain boundaries limiting the contact of grains [26]. Particularly in TiO_2/SiO_2 case, it was suggested that tetrahedral Ti sites are formed in SiO_2 matrix at the interface, and the interaction of these sites with TiO_6 octahedra prevents the phase transformation from anatase to thermodynamically stable phase, rutile [37]. Our analysis, where flame hydrolytic synthesized titania/silica composites are used, showed similar results to previously stated research findings. Figure 3.1.3 shows the positive correlation

between the silica content and the critical temperature at which more than 50 % of transformation was completed for T-series (hydrothermal treatment). The critical temperature for 9.71 % silica doping was accepted as 1050 ^{o}C, which is the midpoint for the observed start (1000 ^{o}C) and completion (1100 ^{o}C) of transformation under annealing conditions of this work.

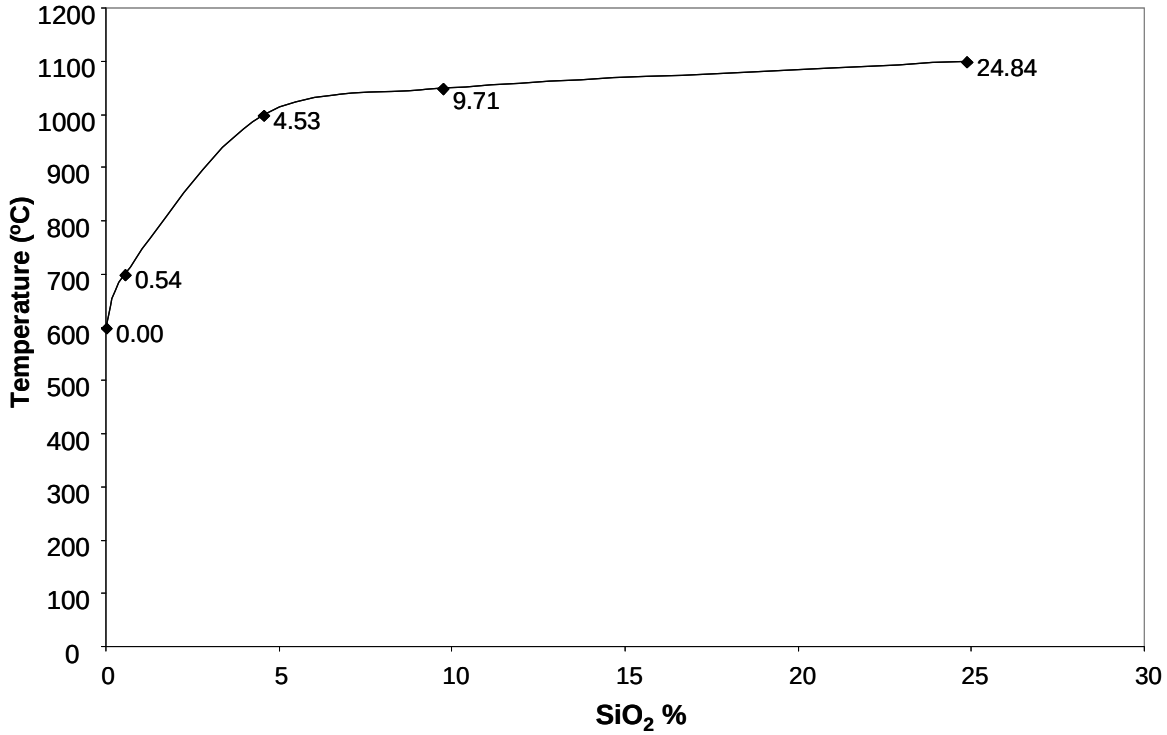

Figure 3.1.3 Change of the critical temperature with SiO_2 %.

For the pure titania sample, the phase transformation from anatase to rutile occurs around 600 ^{o}C, and even the smallest amount of silica doping, e.g. 0.54 %, prevents the phase transformation at that temperature and shifts it to higher values. For 0.54 % silica doping, the start of transformation was shifted to 600-700 ^{o}C and it was complete at 800 ^{o}C. But, as the dopant amount increased to 4.53 %, the start of transformation was

increased even up to 1000 ^{o}C. The complete phase transformation from anatase to rutile takes places at 1200 ^{o}C, for 24.84 % silica content.

Figure 3.1.4 shows the plot of the fraction of the anatase phase as a function of temperature for different silica doping amounts under thermal and hydrothermal conditions. None of the as-prepared TiO_2/SiO_2 nano-sized composites have pure anatase phase, and the fraction of rutile phase varies between 15 and 30 % for different silica contents. This variation is mainly expected to occur as a result of different flame-hydroltic reaction conditions rather than the differing silica contents. It could be discussed that a higher rutile fraction in the as-prepared samples might enhance the transformation of anatase particles into rutile by acting as nucleation centers for the phase transformation. However in our case the effect of silica on the retardation of phase transformation was more prominent. The nano-sized composite having the highest rutile fraction at the beginning, ca. 30 %, still completely transformed into rutile at the highest temperature, 1200 ^{o}C, by having 24.84 % silica content. On the other hand, the lowest rutile fraction, ca. 15 %, for the as-prepared samples was observed for 9.71 % SiO_2 composite. But, its complete transformation into rutile was at 1100 ^{o}C, which is lower than the 24.84 % SiO_2 composite's, proving the importance of silica on suppressing the transformation from anatase to rutile. Also, this can be seen in Figure 3.1.4 as the temperature range for anatase to rutile phase transformation shifted to higher values with the increase of SiO_2 content for both thermal and hydrothermal conditions.

As stated previously and observed by the similar shapes of the curves (Figure 3.1.4 a and b), the critical transformation temperatures, and the anatase-rutile fractions at the temperatures other than the critical ones are very close to each other in thermal and hydrothermal series. However, there is a difference between these series in terms rutile fractions at the critical temperatures.

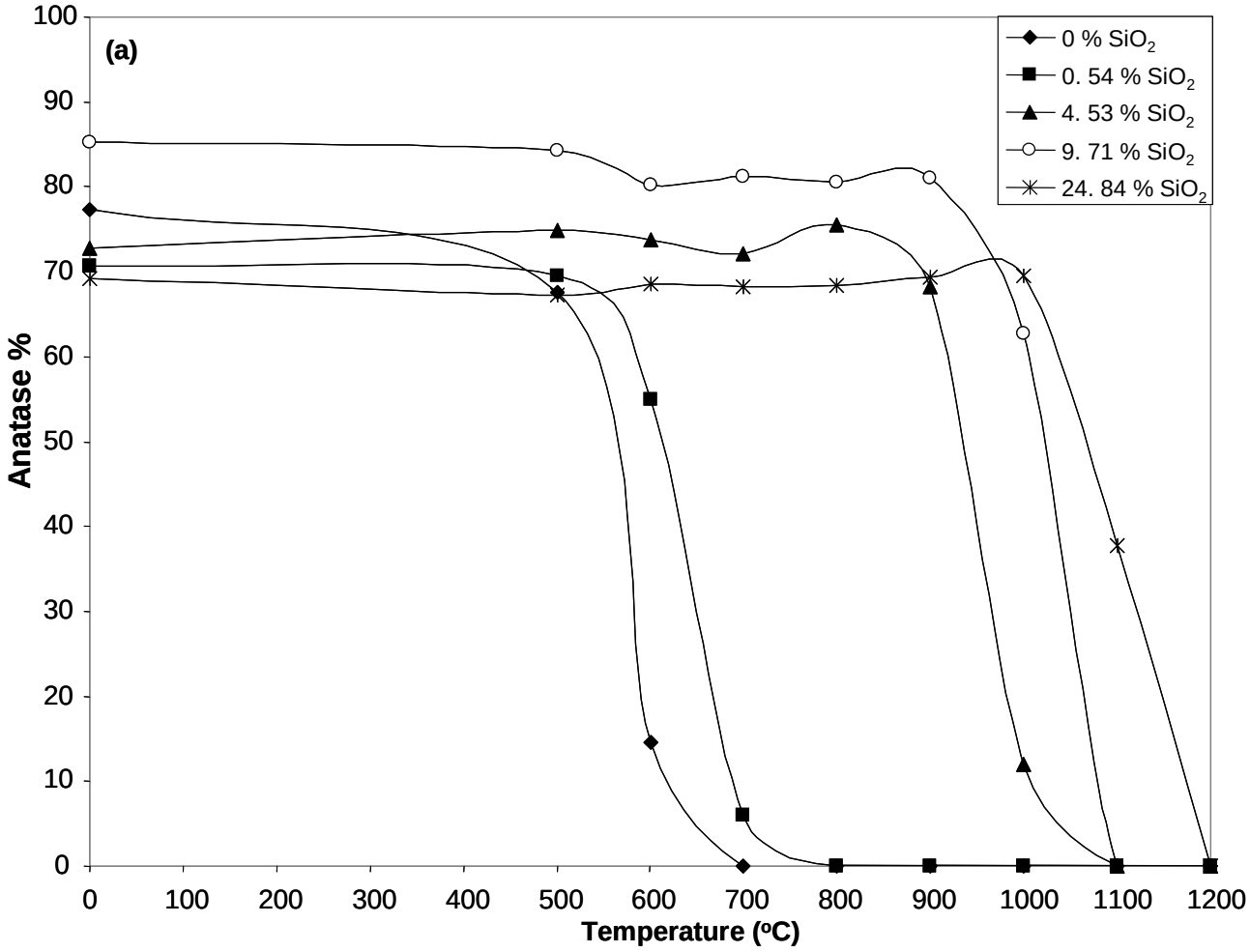

Figure 3.1.4.a Change in anatase fraction with annealing temperature for TiO_2/SiO_2 nano-sized composite series under hydrothermal conditions.

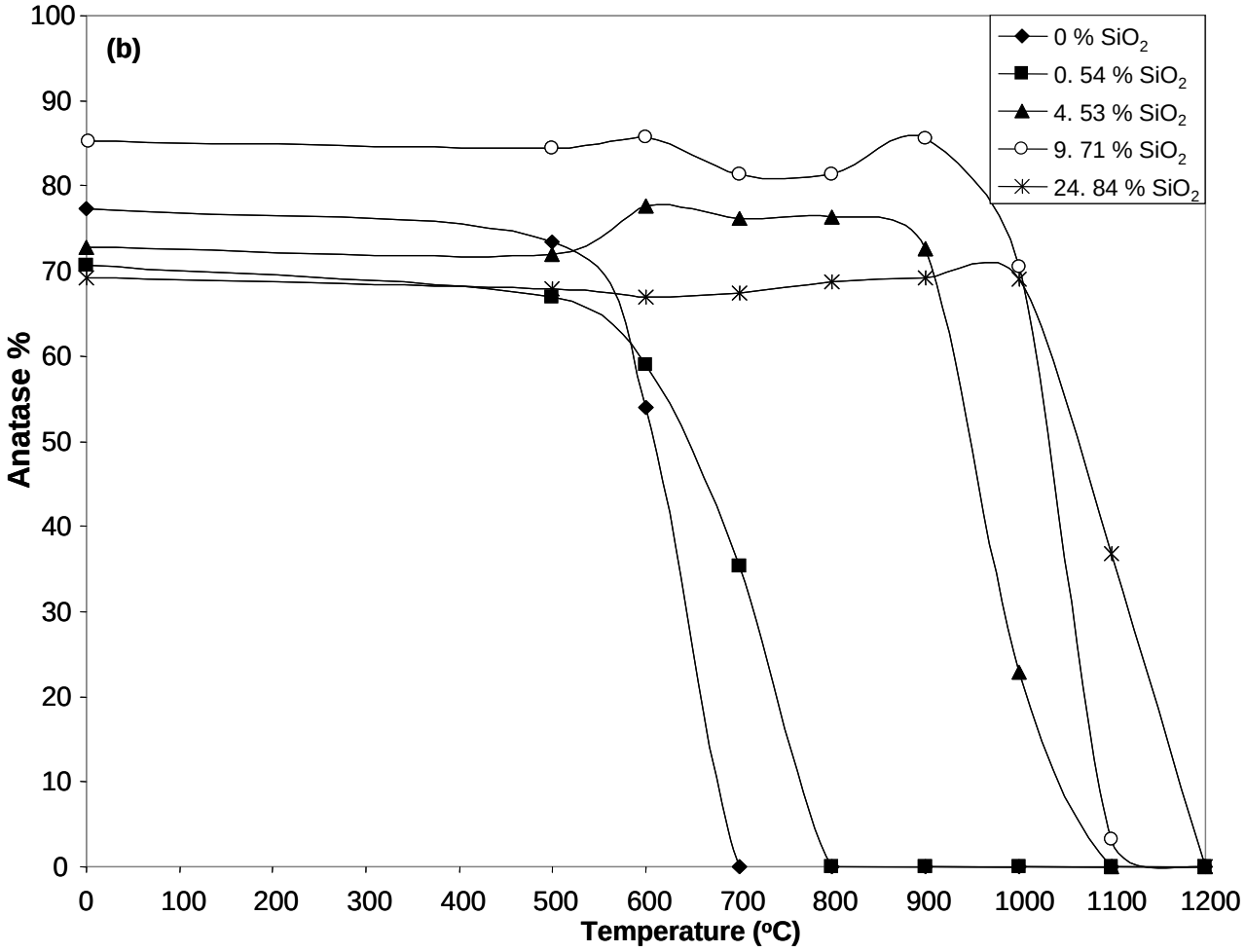

Figure 3.1.4.b Change in anatase fraction with annealing temperature for TiO_2/SiO_2 nano-sized composite series under thermal conditions.

The effect of H_2O atmosphere

According to Shannon et al. [13], the rate of transformation from anatase to rutile is accelerated under H_2 and reducing atmospheres by the formation of oxygen vacancies, and a second phase (Magneli phases Ti_nO_{2n-1}, n = 4, 5,…, 10) that could act as a nucleating agent for the rutile phase. Mackenzie [38] also found similar results and argued that the reaction in a hydrogen atmosphere did not have a different mechanism compared to that in air; however, the transformation in hydrogen is approximately 10 times faster at comparable temperatures. The rate constants he calculated for the anatase-rutile transformation in (5% H_2 / 95% N_2) atmosphere and in air at 970 ^oC were 1.86 x 10^{-4} s^{-1} and 2.0 x 10^{-5} s^{-1}, respectively, whereas the other values, such as Ea(kJ/mole), A(s^{-1}), ΔG^*(kJ/mole) and ΔS^*(J K^{-1}), were identical.

The formation of oxygen vacancies could increase the rate of phase transformation via reducing the strain energy that the oxygen ions need to overcome to occupy their new sites at the rutile phase, and by the less energy required to break Ti-O bonds [13]. It is worth mentioning that our phase analysis results for the samples annealed under hydrothermal conditions are in good agreement with those previously reported showing the effect of reducing atmospheres [13, 29, 38]. We found that the pure titania has 46 % rutile fraction when sintered at 600 ^oC, but increasing to 85 % for annealing under hydrothermal conditions (100 g/m^3 absolute humidity, 600 ^oC). Although a detailed kinetic analysis has not been made in this work, the higher rutile fraction obtained at the same annealing time under H_2O atmosphere is a good indication for the increase in the rate of phase transformation.

Mackenzie [38] also claimed that the steam would accelerate the rate of phase transformation without mentioning any details on the properties of the atmosphere. Here, we suggest that the formation of oxygen vacancies and the rate of phase transformation

from anatase to rutile might be promoted under hydrothermal conditions according to **(1)** (□ = Oxygen vacancy in TiO_2 lattice)**.**

$$\begin{array}{l} \xrightarrow{\Delta T} \\ 2H_2O_{(g)} \rightarrow\ 2H^+ + 2OH^- \\ O^{2-} + 2H^+ \rightarrow H_2O_{(g)} + \square \end{array} \qquad \textbf{(1)}$$

The partial reduction of TiO_2 and the formation of anion vacancies under H_2O atmosphere are also confirmed in our experiments by the darker color of samples that were annealed under hydrothermal conditions (Figure 3.1.5).

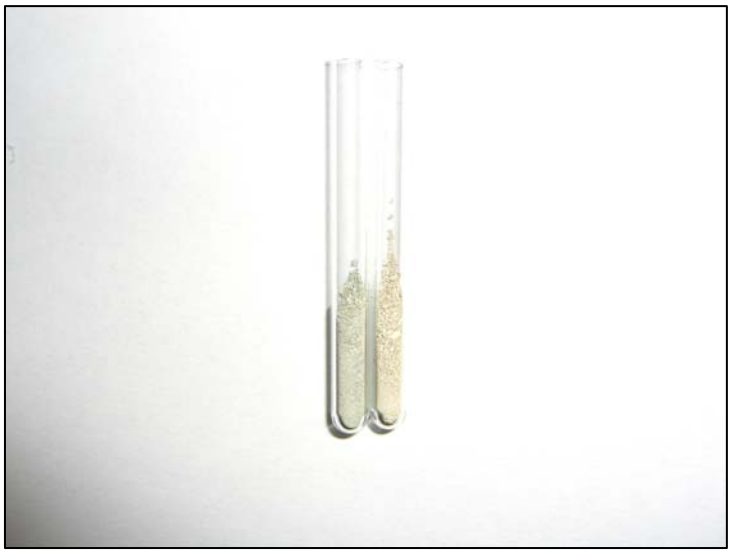

Figure 3.1.5 0.54 % SiO_2 sample annealed at 1100 ^oC under thermal (right) and hydrothermal conditions (left).

Magneli phases ($Ti_nO_{2n\ -1}$, n = 4, 5,…, 10) occurring at high temperatures were suggested to have gray-blue colors [39], and could be responsible for the darker colors of

hydrothermal treated samples. Another reason for the color difference could be the mixed valency (Ti^{3+}/Ti^{4+}) stemming from the reduction of Ti^{4+} to Ti^{3+} in order to balance the charge as oxygen vacancies are formed. Similar observations about the color under the reducing atmospheres were also reported by Shannon [13] and Mackenzie [38] claiming the formation of Magneli phases acting as nucleation centers for the explanation of kinetic facts. The stated similarities between the reducing atmospheres and H_2O atmosphere further support that the rate of transformation from anatase to rutile was elevated under hydrothermal conditions.

Despite the difference of ca. 40 % in rutile content between the pure titania samples heated under thermal and hydrothermal conditions at the critical transformation temperature, this value was decreased to 0-10 % as the SiO_2 % has increased (Figure 3.1.4). The stated phenomenon for TiO_2/SiO_2 systems can again be explained by the accumulation of SiO_2 at the grain boundaries limiting the grain growth and the crystallite size of anatase TiO_2. SiO_2 at the grain boundaries of TiO_2 might not have only thermodynamic influences on the phase transformation from anatase to rutile but it might have also affected the reaction kinetics by inhibiting the contact of different anatase particles and slowing the nucleation.

Crystallite sizes

The Table 3.1.3 shows the average crystallite sizes of the anatase particles in TiO_2/SiO_2 composites heated under hydrothermal conditions. The particle size observed by TEM for the as-prepared TiO_2 with 0% silica agrees well to the crystallite size estimated from the line broadening of the XRD peak (Figure 3.1.6).

Table 3.1.3 The average anatase crystallite size (nm) for TiO_2/SiO_2 series annealed at different temperatures under hydrothermal conditions.

Sample SiO_2%	As-prepared	500 °C	600 °C	700 °C	800 °C	900 °C	1000 °C	1100 °C	1200 °C
0%	21.4	23.3	35.4	rutile	rutile	rutile	rutile	rutile	rutile
0.54	15.1	16.3	19.9	35.4	rutile	rutile	rutile	rutile	rutile
4.53 %	15.7	14.5	14.3	13.6	14.5	16.0	24.7	rutile	rutile
9.71 %	11.0	11.0	11.8	11.5	11.3	12.9	20.4	rutile	rutile
24.84 %	13.4	13.6	13.1	13.1	13.6	13.8	17.7	27.1	rutile

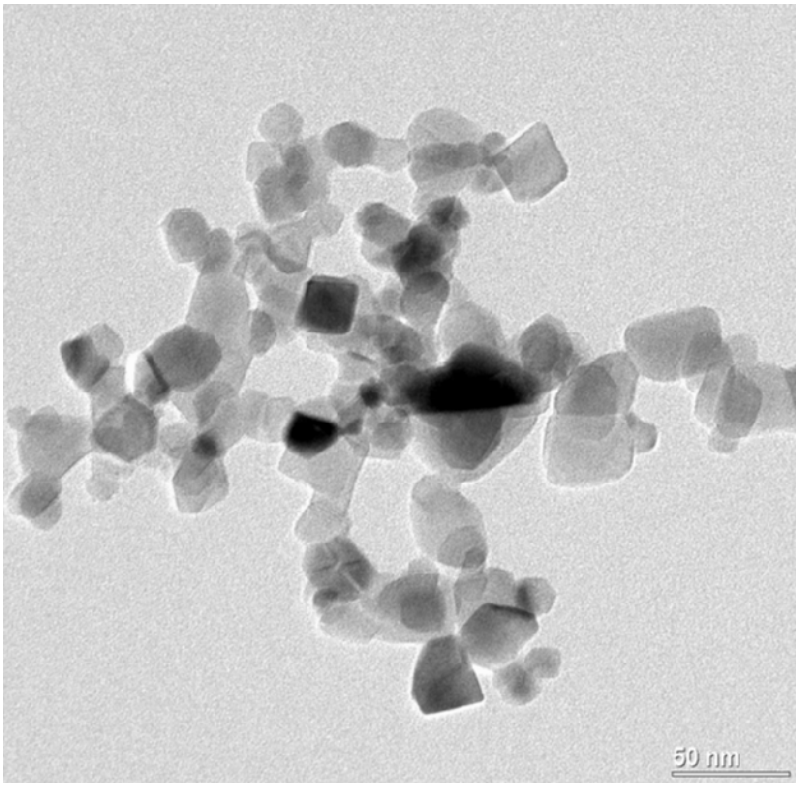

Figure 3.1.6 TEM image of as-prepared TiO_2, 0 % silica [40].

Zhang and Banfield's theoretical studies [20] showed that there is a critical size, ca. 14 nm, for the phase stability of TiO_2. The rutile is the thermodynamically favored phase for particle sizes above and a crossover for the phase stability occurs at the critical size. Besides, in situ TEM studies, Hyoung Lee et al. [41] observed that anatase crystallites coalesce by heating and the large anatase crystallites transforms into rutile upon reaching a critical size. Once rutile crystallite is nucleated, it grows by absorbing the neighboring anatase and the process continues to the disappearance of nearby anatase particles. Y. Hu et al. [42] also found that the critical size needed to be reached for the phase transformation from anatase to rutile was around 15 nm. Our analysis on the crystallite size is in good agreement with those reported and shows that the anatase crystallites grow upon heating and transform into rutile after reaching a critical size. The change in average anatase crystallite size with annealing temperature for TiO_2/SiO_2 nano-sized composite series under hydrothermal conditions is illustrated in Figure 3.1.7. The anatase crystallite sizes are quite constant until reaching the critical transformation temperatures (Figure 3.1.3), at which they have grown considerably, exceeded the critical size and transformed into rutile.

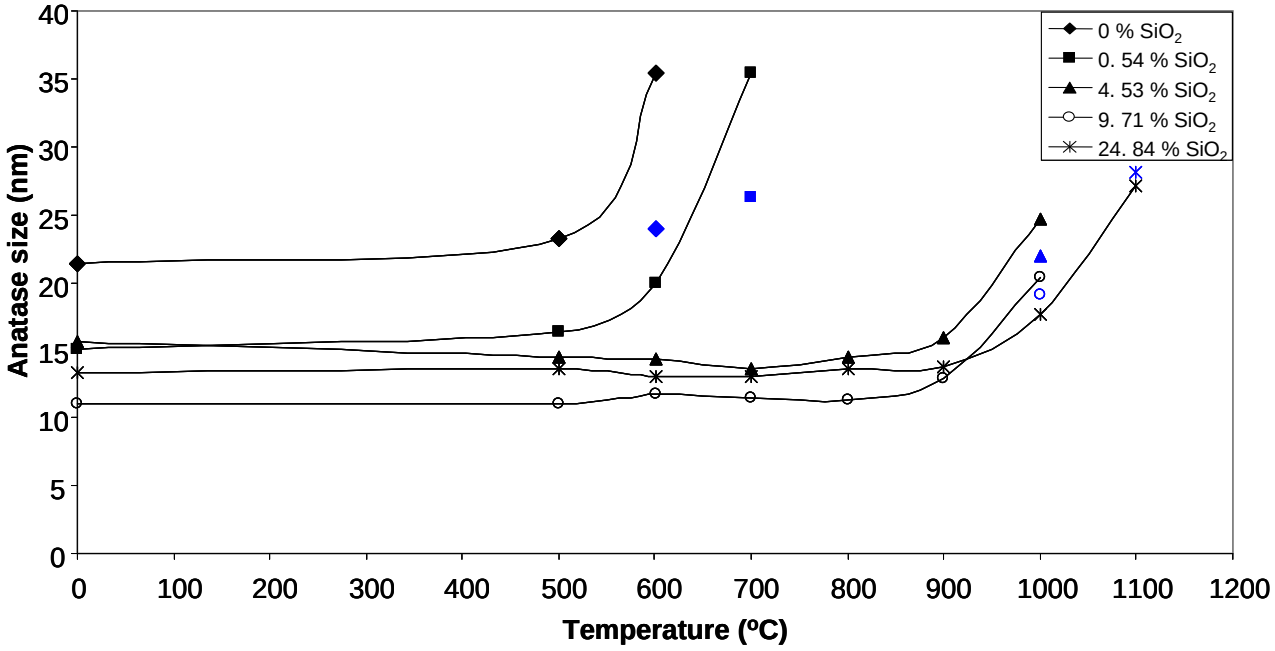

Figure 3.1.7 Change in average anatase crystallite size with annealing temperature for TiO_2/SiO_2 nano-sized composite series under hydrothermal conditions. Blue labels show the corresponding average anatase crystallite sizes of thermal treated samples (M-series) at the critical temperatures.

As it can be seen from the right shift of the curves (Figure 3.1.7), the presence of SiO_2 restrains the growth of anatase grains and can keep them under the critical size up to 1000-1100 ^oC for 4.53, 9.71 and 24.84 % doping amounts. These findings harmonize well with our phase analysis results and the aforementioned theoretical studies [20, 41].

Furthermore, when the anatase crystallite sizes of thermal and hydrothermal treated samples at the critical temperatures are compared, it can be seen that there is a difference of ca. 10 nm for the undoped titania, which decreases to ca. 1-2 nm as the SiO_2 content has increased. These findings agree well to the rutile fraction differences we observed between

M-series and T-series, as Y. Hu et al. [42] also reported a linear correlation between the average size of the anatase and percent transformation to rutile.

Here, we showed that there is a positive correlation between the silica content and the phase stability of anatase for the flame-hydrolytic synthesized titania tested under thermal and hydrothermal conditions. Previous literature and research results also revealed that an optimum amount of silica content can suppress the phase transformation from rutile to anatase for sol-gel synthesized titania, under thermal conditions [4, 14, 25]; yet, our results confirm these findings even in harsher hydrothermal conditions.

3.2 Raman characterization:

It is possible to verify the phase transition information for TiO_2/SiO_2 nano-sized composites by Raman Spectroscopy. Figure 3.2.1 shows the observed Raman spectra of the pure anatase and rutile phases that correspond well with the literature data [14, 18, 25]. The main bands for anatase are observed at 145, 197, 397, 518 and 641 cm^{-1}, and for rutile at 143, 235, 449 and 610 cm^{-1}.

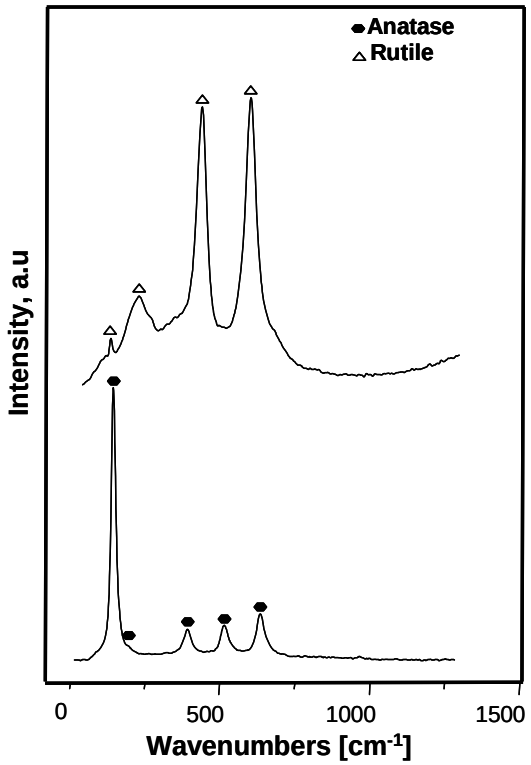

Figure 3.2.1 Raman spectra of the pure anatase and rutile TiO_2.

The Raman spectra of test samples as-prepared and at differing critical transformation temperatures under thermal and hydrothermal conditions are illustrated in Figure 3.2.2 series. The phase transformation from anatase to rutile can be clearly seen as the sharp peak of anatase at 145 cm^{-1} disappears and the rutile bands at 449 and 610 cm^{-1} emerge (Figure 3.2.2.a). The difference in the phase fractions (anatase and rutile) between the M-series and T-series of 0, 0.54 and 4.53 % SiO_2 samples are also observable from varying intensities of Raman bands (Figure 3.2.2.a, b, c). For 9.71 and 24.84 % silica doped samples, the results of the Raman spectra of thermal and hydrothermal treated samples at the critical temperatures are directly comparable with each other, which is consistent with XRD measurements in terms of having a low difference in rutile fraction (Figure 3.2.2.d, e).

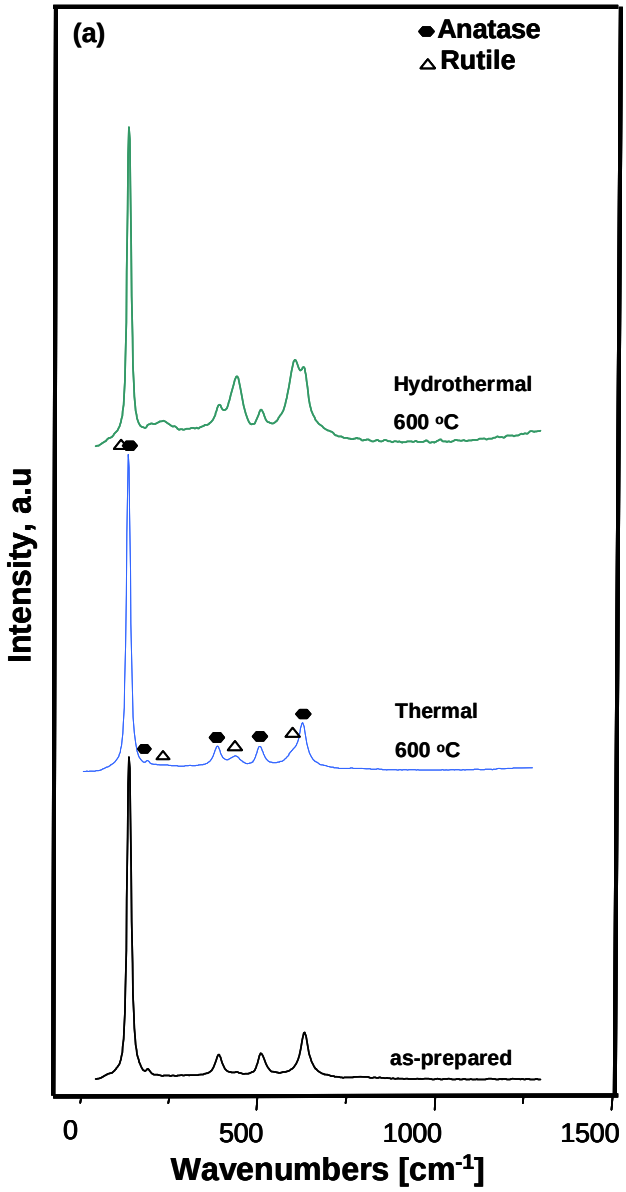

Figure 3.2.2.a Raman spectra of TiO_2 with 0 % silica content, as-prepared and at phase transformation temperatures under thermal and hydrothermal conditions.

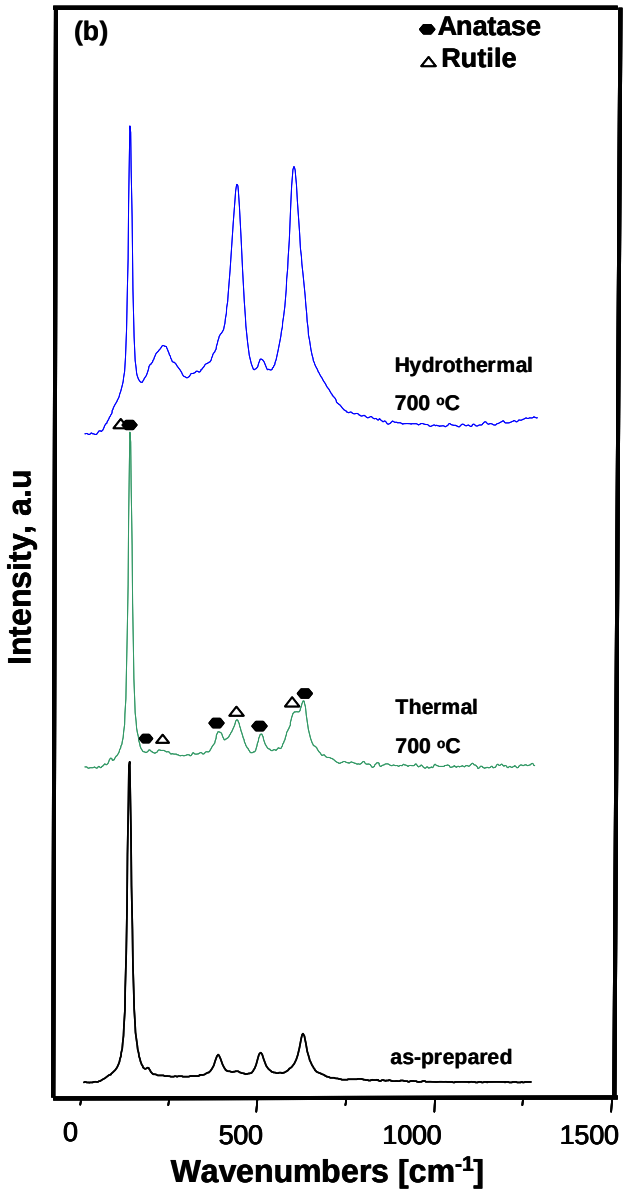

Figure 3.2.2.b Raman spectra of TiO_2 with 0.54 % silica content, as-prepared and at phase transformation temperatures under thermal and hydrothermal conditions.

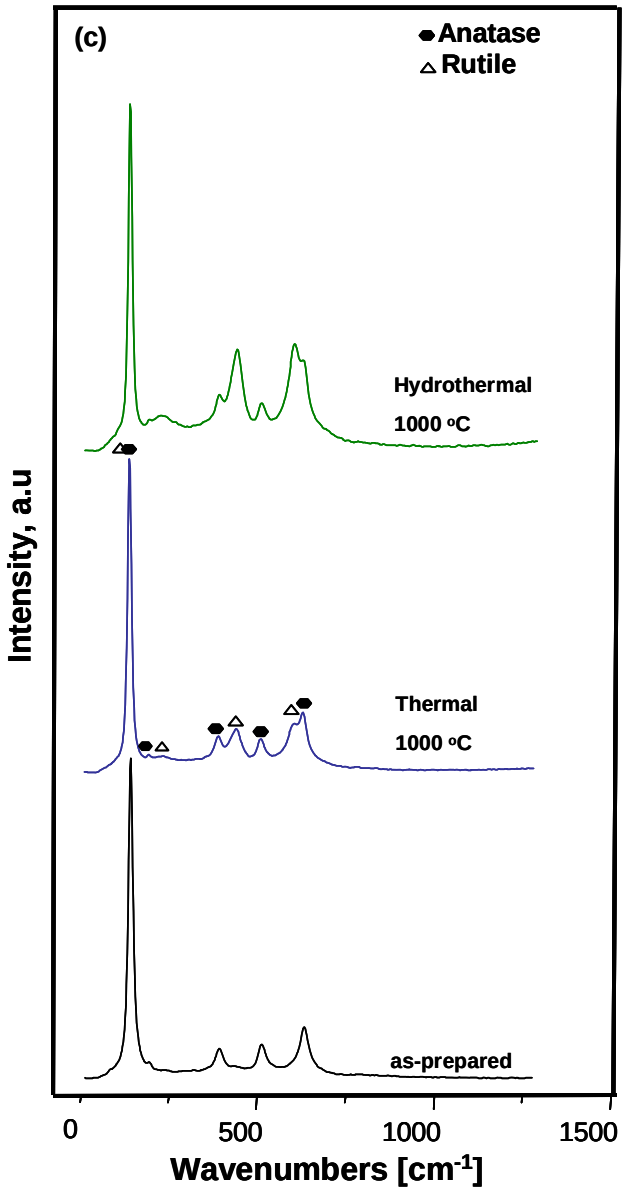

Figure 3.2.2.c Raman spectra of TiO_2 with 4.53 % silica content, as-prepared and at phase transformation temperatures under thermal and hydrothermal conditions.

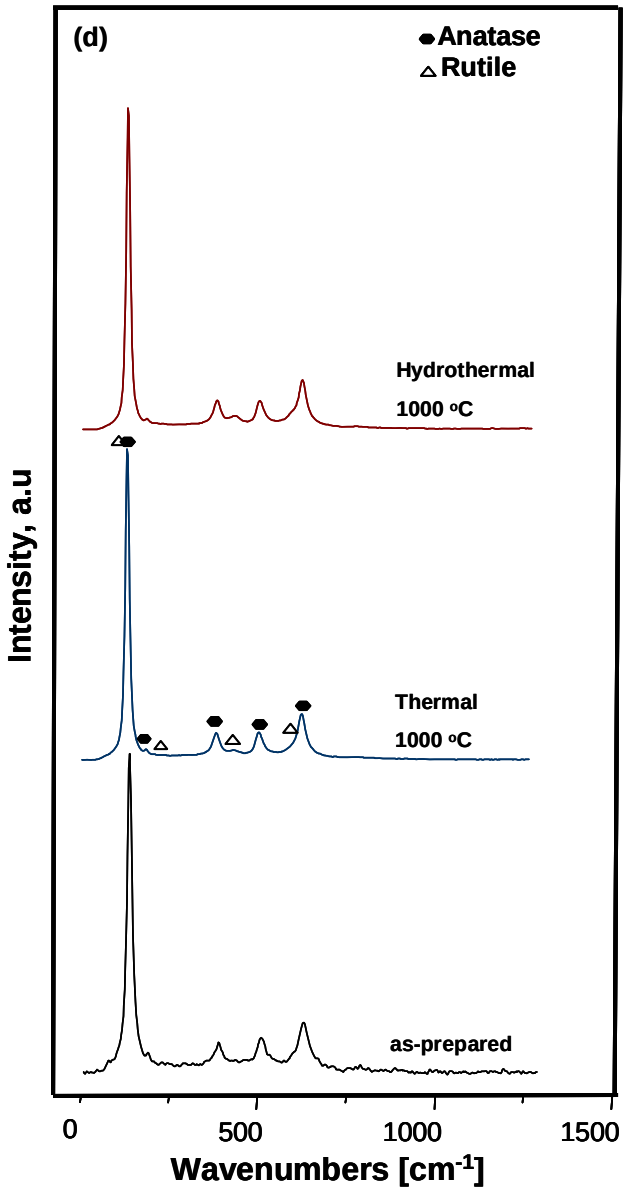

Figure 3.2.2.d Raman spectra of TiO_2 with 9.71 % silica content, as-prepared and at phase transformation temperatures under thermal and hydrothermal conditions.

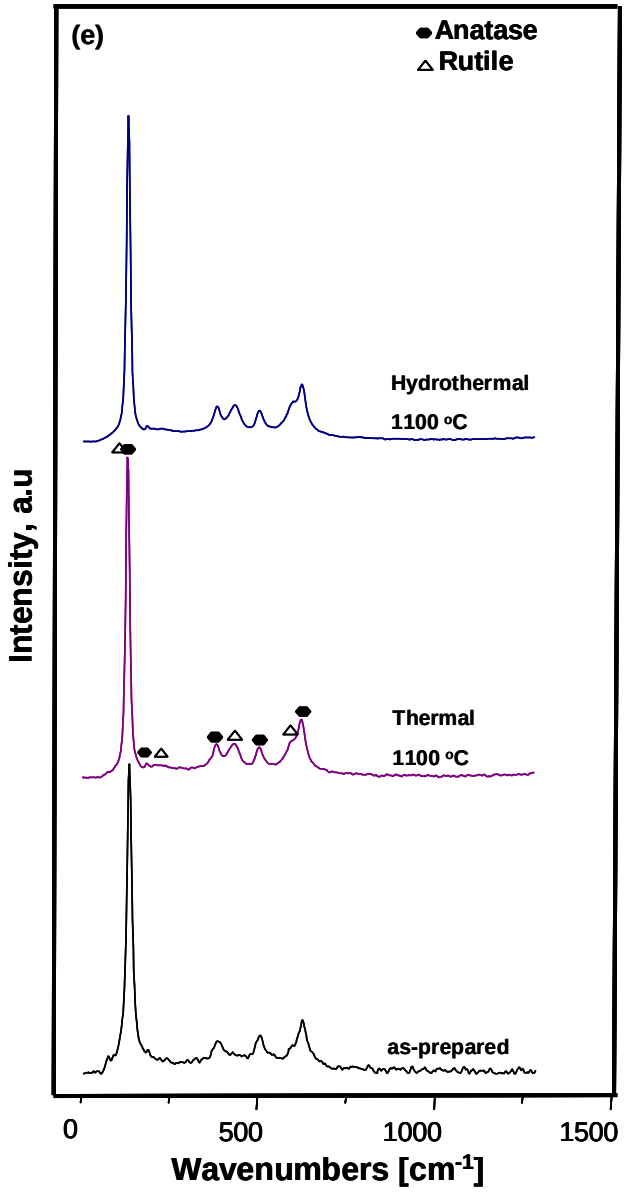

Figure 3.2.2.e Raman spectra of TiO_2 with 24.84 % silica content, as-prepared and at phase transformation temperatures under thermal and hydrothermal conditions.

The phase transformation temperatures and differing phase contents, which were determined by XRD powder characterization, are here confirmed by Raman Spectroscopy. Additionally, our raman characterization of TiO_2/SiO_2 samples supports that SiO_2 does not exist as a separate amorphous phase in the composites. According to Hirano et al. [14], in the presence of amorphous SiO_2, weak intensity, broadened peaks and relatively high background were observed for the TiO_2/SiO_2 composites they studied (Figure 3.2.3).

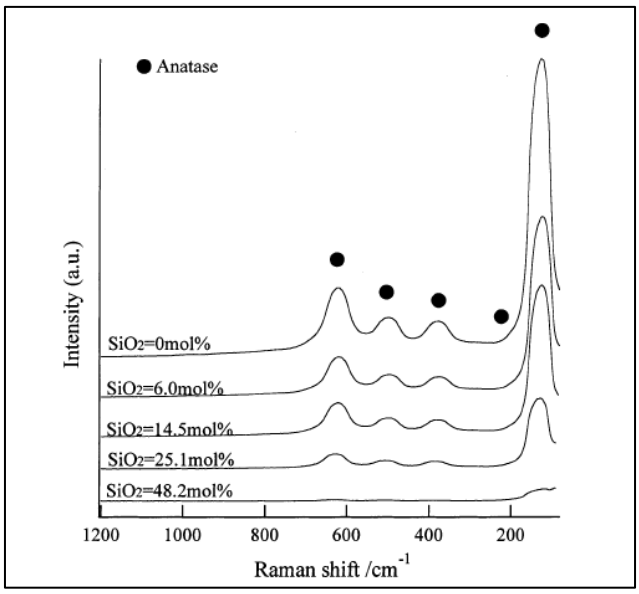

Figure 3.2.3 Raman spectra of as-prepared TiO_2/SiO_2 composite nanoparticles from the studies of Hirano et al. [14].

Similarly, R. Jossen et al. [18] found a higher background in the raman spectra of "flame-made silica-vanadia-tungsten oxide-titania" for increasing silica content. However, in our studies, such increases in the background or broadening of peaks are not observed in the raman spectra of samples, even for the highest SiO_2 content, 24.84 % (Figure 3.2.2.e).

This result indicates that most of the silica doesn't exist separately as an amorphous phase in the flame hydrolytic synthesized TiO_2/SiO_2 nano-sized composites, and is in interaction with titania particles by various mechanisms, such as Ti-O-Si bonding at the grain boundaries and the substitution of Ti^{4+} (0.061 nm) by Si^{4+} (0.040 nm) [43]. The enhanced properties and phase stability of TiO_2/SiO_2 nano-sized composites are also ascribed to these interactions as it is demonstrated and discussed in sections 3.1 and 3.3.

3.3 BET characterization:

BET surface areas of TiO_2/SiO_2 nano-sized composites calcined at 500, 600, 700, 800, 900 and 1000 ^oC under thermal and hydrothermal conditions are listed in Table (3.3.1 & 3.3.2).

Table 3.3.1 BET surface area (m^2/g) of TiO_2/SiO_2 series under hydrothermal conditions at different temperatures.

Sample SiO_2%	As-prepared	500 ^oC	600 ^oC	700 ^oC	800 ^oC	900 ^oC	1000 ^oC
0%	52	41	18	8	2	0	0
0.54	86	66	52	31	17	10	3
4.53 %	102	96	94	90	86	76	25
9.71 %	130	119	115	114	108	93	40
24.84 %	104	96	95	91	86	82	57

Table 3.3.2 BET surface area (m^2/g) of TiO_2/SiO_2 series under thermal conditions at different temperatures.

Sample SiO_2%	As-prepared	500 ^oC	600 ^oC	700 ^oC	800 ^oC	900 ^oC	1000 ^oC
0%	52	46	33	9	2	0	0
0.54	86	75	56	31	15	10	5
4.53 %	102	97	95	90	82	67	32
9.71 %	130	124	119	115	109	96	50
24.84 %	104	101	99	94	88	82	64

As the calcination temperature increases, the BET surface area of all samples decreases; however it can be seen that an effective amount of silica can diminish the rate of decrease.

The pure titania sample reaches the value of 0 m^2/g BET surface area at 900 ^oC, but the composite with 0.54 % silica has a BET surface area of 10 m^2/g at the same temperature. Furthermore, 24.84 % SiO_2 doped titania sample has the highest surface area, 57 m^2/g, at 1000 ^oC under hydrothermal conditions and maintains 55 % of its initial surface area. At the same conditions, the BET surface areas are 40, 25, 3 m^2/g for 9.71, 4.53, 0.54 % SiO_2 doping amounts, respectively.

It has been previously reported that SiO_2 doping can increase the surface area of titania by introducing defects, and keep it at high temperatures via Ti-O-Si bonding [18, 25]. Our results corroborated this finding and showed that there is a direct relationship between the amount of silica and the retained BET surface after annealing (Figure 3.3.1).

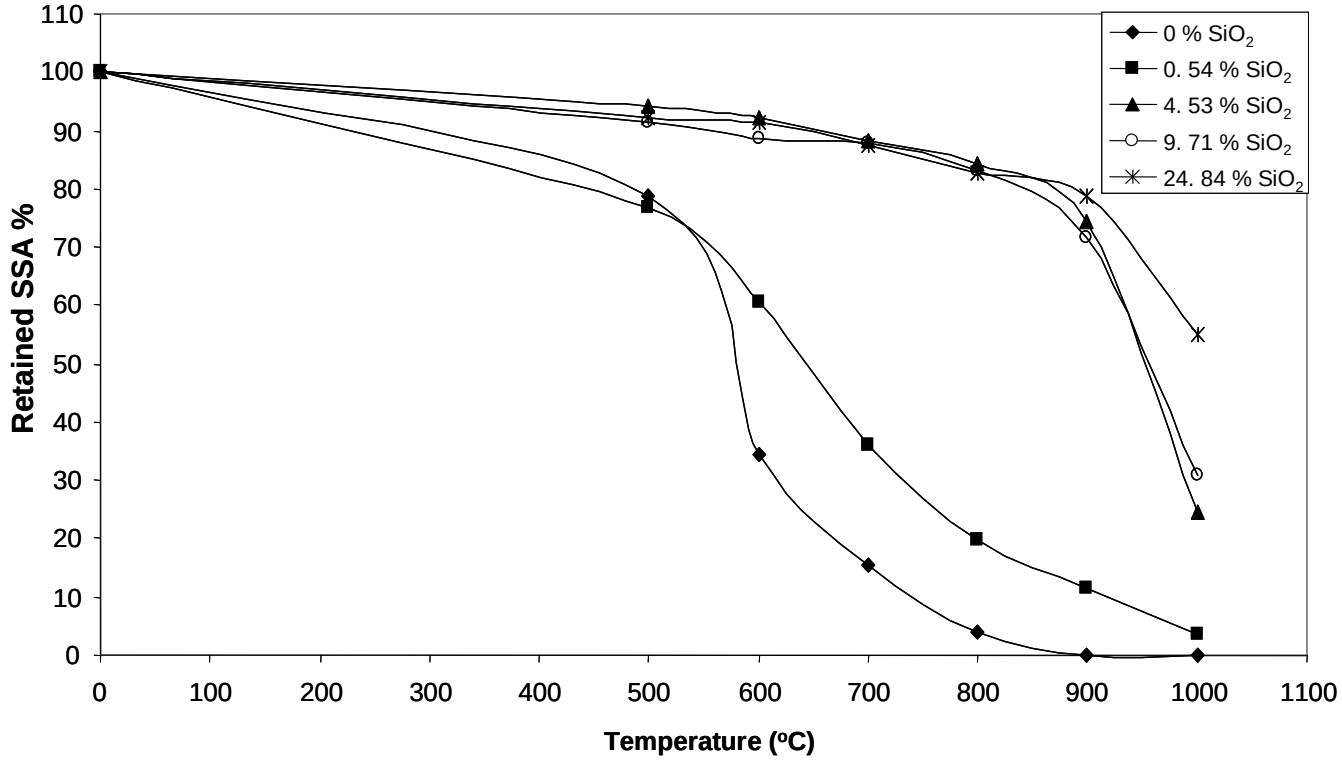

Figure 3.3.1 BET surface area retained after annealing under hydrothermal conditions plotted against heating temperature.

Besides, when T-series (hydrothermal treatment) and M-series (thermal treatment) are compared, it is found that M-series have larger BET surface area values, especially at the corresponding phase transformation temperatures (Table 3.3.1 & 3.3.2). This finding might be a result of differing rutile fractions between M and T series. Hyoung Lee et al. found that the rutile had much lower number of pores compared to anatase by in situ TEM observations [41]. Besides, as it was shown in a number of different studies the average crystallite size of rutile TiO_2 is larger than anatase TiO_2 [4, 18, 41]. Figure 3.3.2, from the studies of Hyoung Lee et al., shows the pore morphology of anatase and rutile particles.

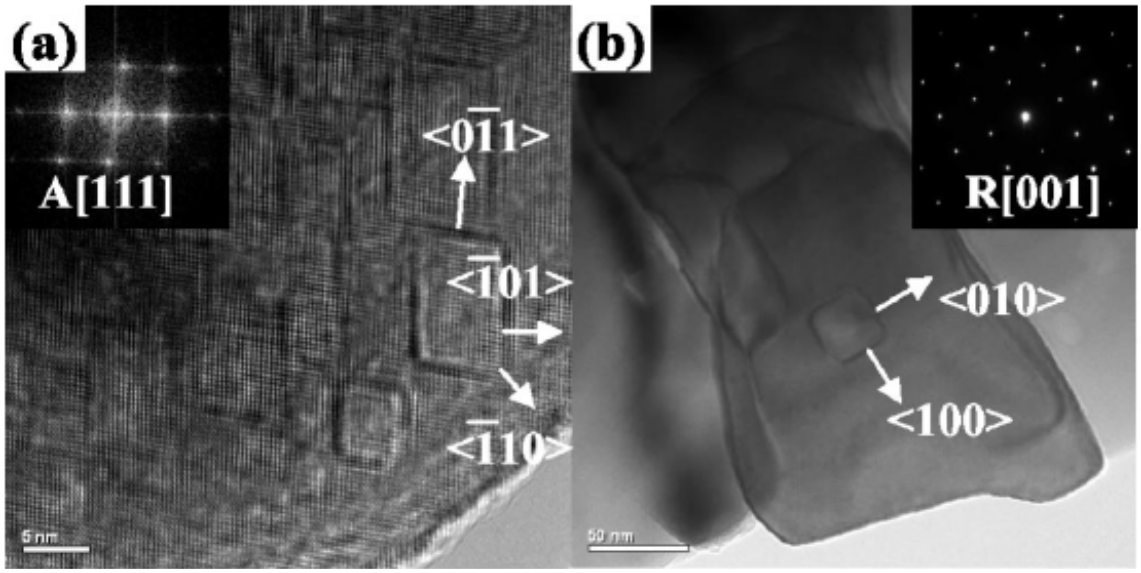

Figure 3.3.2 TEM images showing the pore morphology (a) anatase, (b) rutile [41].

Thus, it can be explained that since M-series have higher anatase fraction at the critical phase transition temperatures, they would have more pores and larger BET surface area compared to T-series. Also, the sharp decrease in the preserved BET surface area % once

the phase transformation from anatase to rutile occurs further supports this explanation. For instance, the pure titania's preserved BET surface area % under hydrothermal conditions dropped off from 79 % at 500 ^{o}C to 35 % at its phase transformation temperature, 600 ^{o}C (Figure 3.3.1). In addition, 0.54 % SiO_2 composite has only 36 % of its initial BET surface area at 700 ^{o}C, whereas the other titania composites with higher silica contents, having not transformed into rutile yet, retain ca. 90 % of their initial surface area values at 600 and 700 ^{o}C . These findings prove the positive influence of SiO_2 addition in maintaining the BET surface area of flame hydrolytic synthesized titania at high temperatures, and agree well with XRD results in terms of the phase transformation temperatures and the effect of hydrothermal conditions.

Chapter 4

CONCLUSION

The phase stability of the flame hydrolytic synthesized TiO_2/SiO_2 nano-sized composites under both thermal and hydrothermal conditions was studied by means of X-ray Powder Diffraction, Raman Spectroscopy and BET surface area measurements. The rate of transformation from anatase to rutile was most likely increased under hydrothermal conditions as it was found out that there is a difference about 40 % in rutile content between the pure titania (Degussa P 25) samples annealed under thermal and hydrothermal conditions at the critical transformation temperature (600 ^oC) for the same time. This difference was attributed to the formation of anion vacancies and the partial reduction of TiO_2 under H_2O atmosphere. The darker color of samples tested under hydrothermal conditions further supported this discussion and was another confirmation for the similarity between H_2O atmosphere and reducing atmospheres, which increase the rate of transformation from anatase to rutile.

Raman spectroscopy confirmed the phase analysis information by distinct intensity differences of rutile and anatase peaks. In addition, raman spectra of samples with high silica content did not have an increased background compared to undoped titania. This observation showed that there was no separate amorphous SiO_2 present in TiO_2/SiO_2 nano-sized composites.

The silica addition into titania matrix decreased the difference between hydrothermal and thermal conditions, and increased the phase transformation temperature and retain the

BET surface area by limiting the growth of titania grains. The average anatase crystallite sizes calculated from the line broadening of XRD peaks supported this discussion revealing the particle sizes smaller than the critical 13-16 nm size for silica doped samples at high temperatures. TiO_2/SiO_2 nano-sized composite having the lowest amount of silica, 0.54 %, still completely transformed into rutile at a temperature higher than 100 ^oC compared to undoped titania. Also, it had a BET surface area of 10 m^2/g at 900 ^oC, which was 0 m^2/g for undoped titania. The stated advantages further increased with higher silica contents and reached maximum for the highest amount of SiO_2 content discussed in this study. The complete phase transformation temperature, 1200 ^oC, and the preserved BET surface area at 1000 ^oC, 57 m^2/g was the highest for 24.84 mol % SiO_2 containing nano-sized composite.

24.84 mol % SiO_2 containing nano-sized composite also had the highest rutile fraction, ca. 30 %, among the as-prepared samples of flame hydrolytic synthesized TiO_2/SiO_2 nano-sized composites. This fact might be considered as a negative effect for the phase stability of anatase fraction. But still, as it was stated, the retarding effect of silica on the phase transformation was more prominent, and the highest complete phase transformation temperature was recorded for 24.84 % SiO_2 composite, though the other composites had lower rutile fractions at the beginning.

Furthermore, it was also discovered that T-series usually have lower BET surface area compared to M-series, and there is a drastic drop of BET surface area as the phase transformation from anatase to rutile occurs, which could be both attributed to lower number of pores and larger grains in rutile TiO_2.

Finally, 5 different mixed oxide systems were annealed at 8 different temperatures under both hydrothermal and thermal conditions; so that the phase analysis of 85 test samples were done in this thesis work. The results obtained from different characterization

methods supported each other in various ways proving the discussed effects of hydrothermal conditions, and SiO_2 doping on the phase stability of titania.

APPENDIX A

XRD PATTERNS OF TiO_2/SiO_2 NANO-SIZED COMPOSITES ANNEALED UNDER HYDROTHERMAL CONDITIONS AT 500, 600, 700, 800, 900, 1000, 1100 and 1200 ^oC

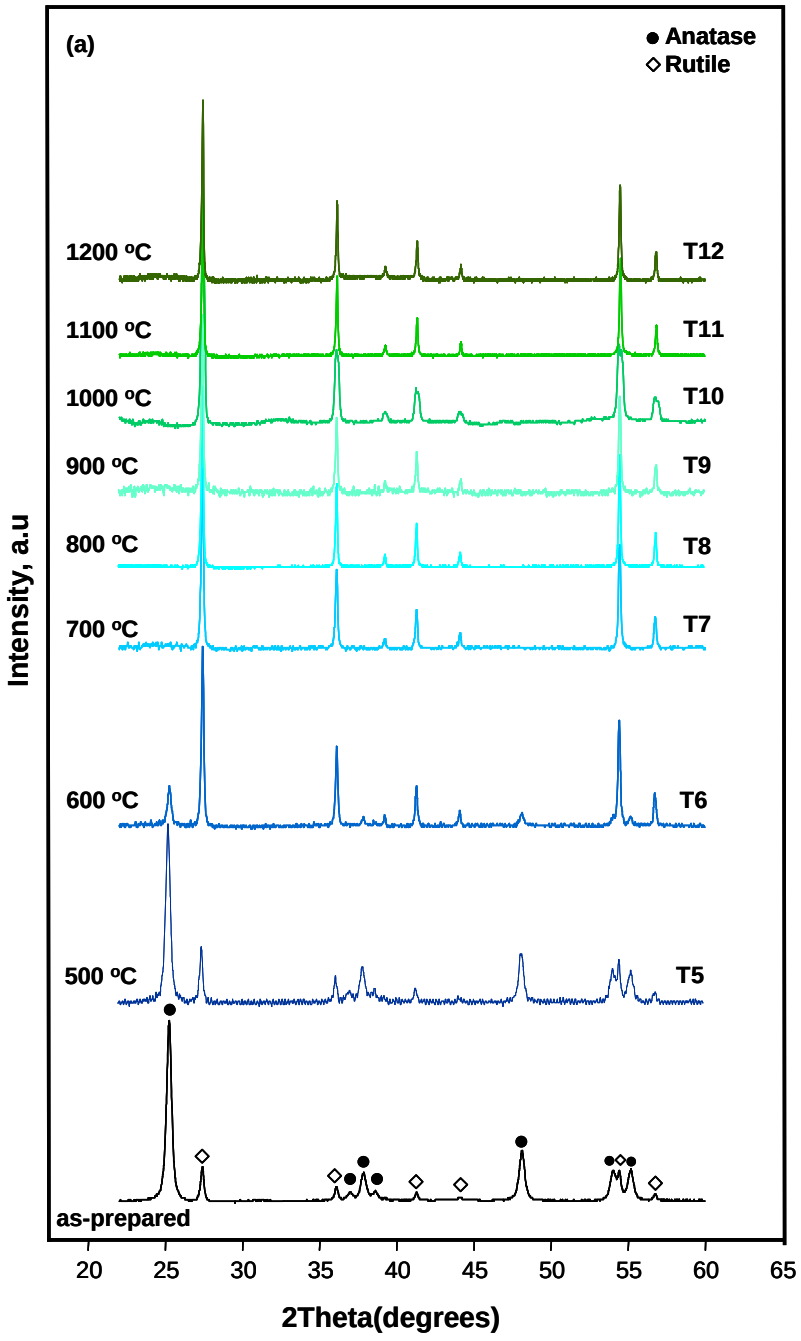

Figure A.a XRD patterns of TiO_2 with 0 % silica content, annealed under hydrothermal conditions.

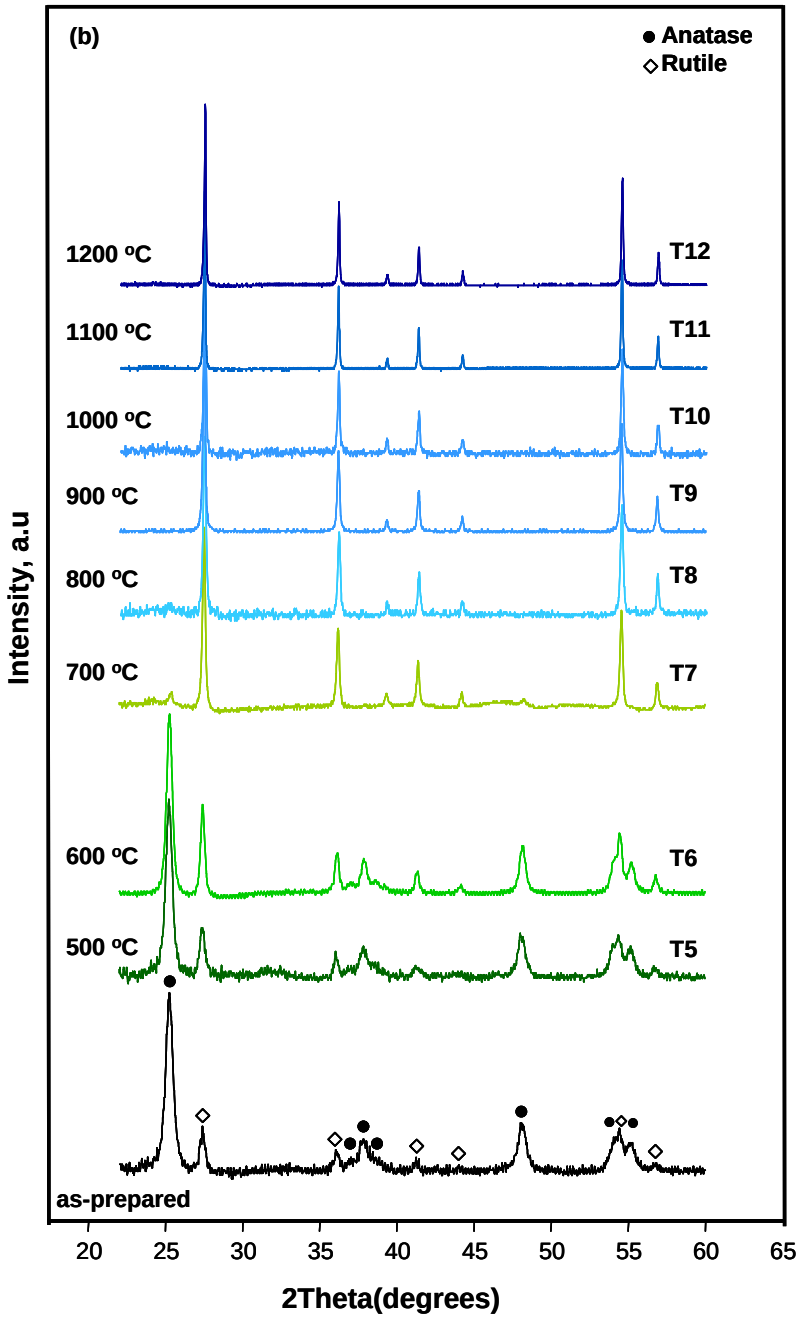

Figure A.b XRD patterns of TiO_2 with 0.54 % silica content, annealed under hydrothermal conditions.

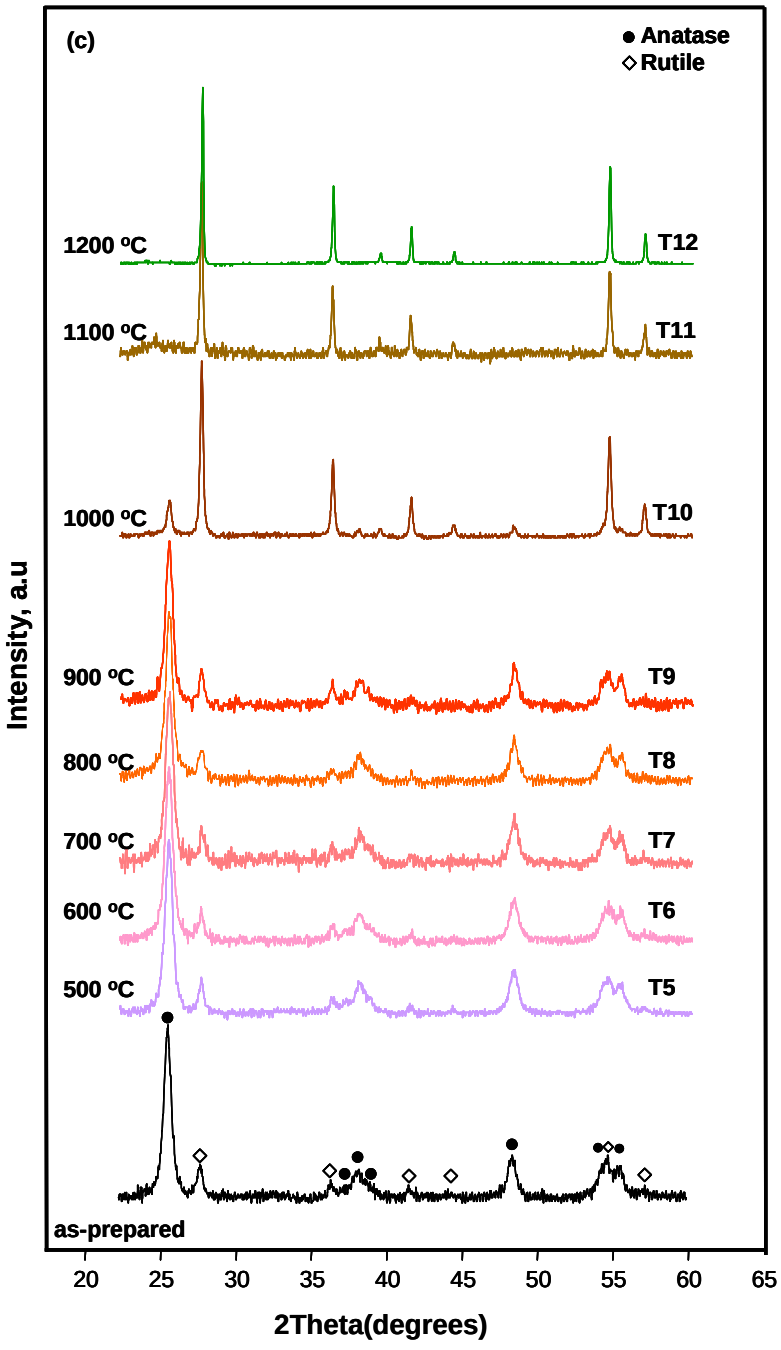

Figure A.c XRD patterns of TiO_2 with 4.53 % silica content, annealed under hydrothermal conditions.

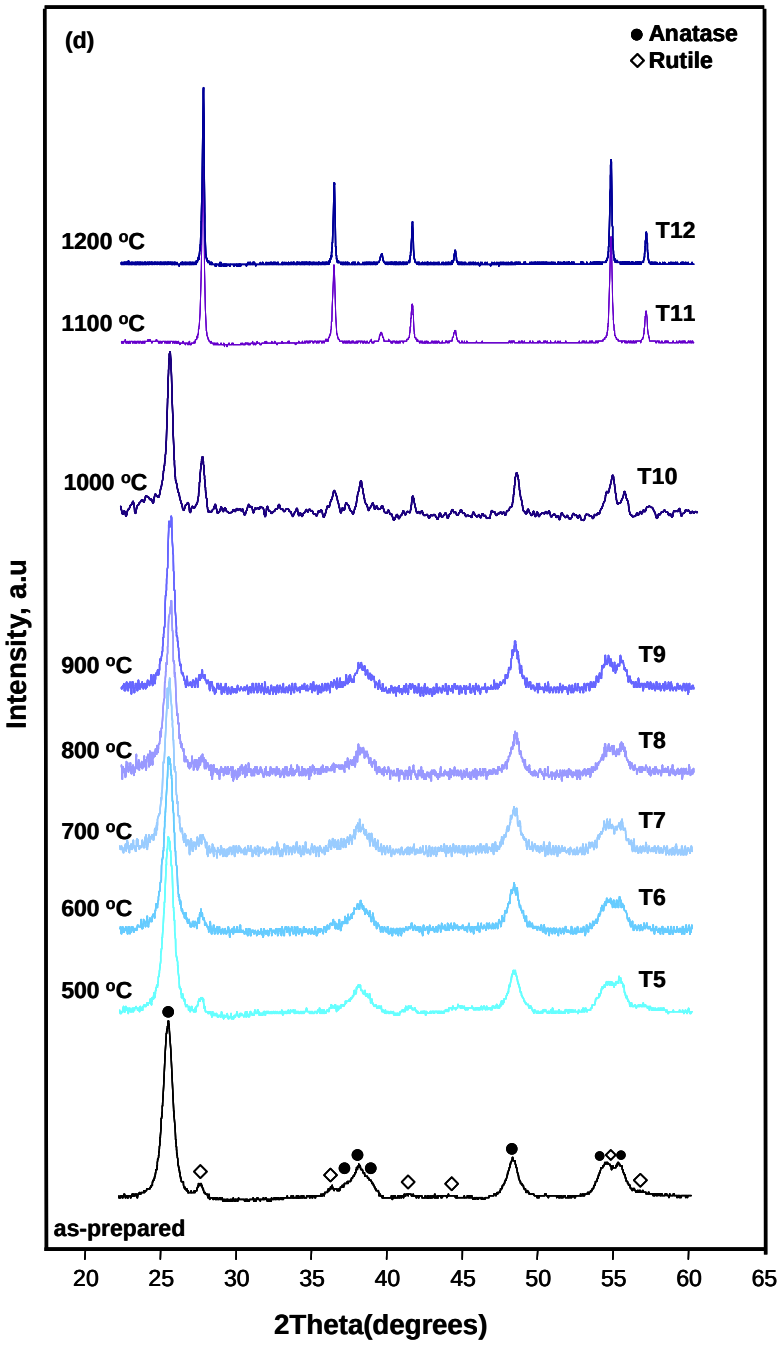

Figure A.d XRD patterns of TiO_2 with 9.71 % silica content, annealed under hydrothermal conditions.

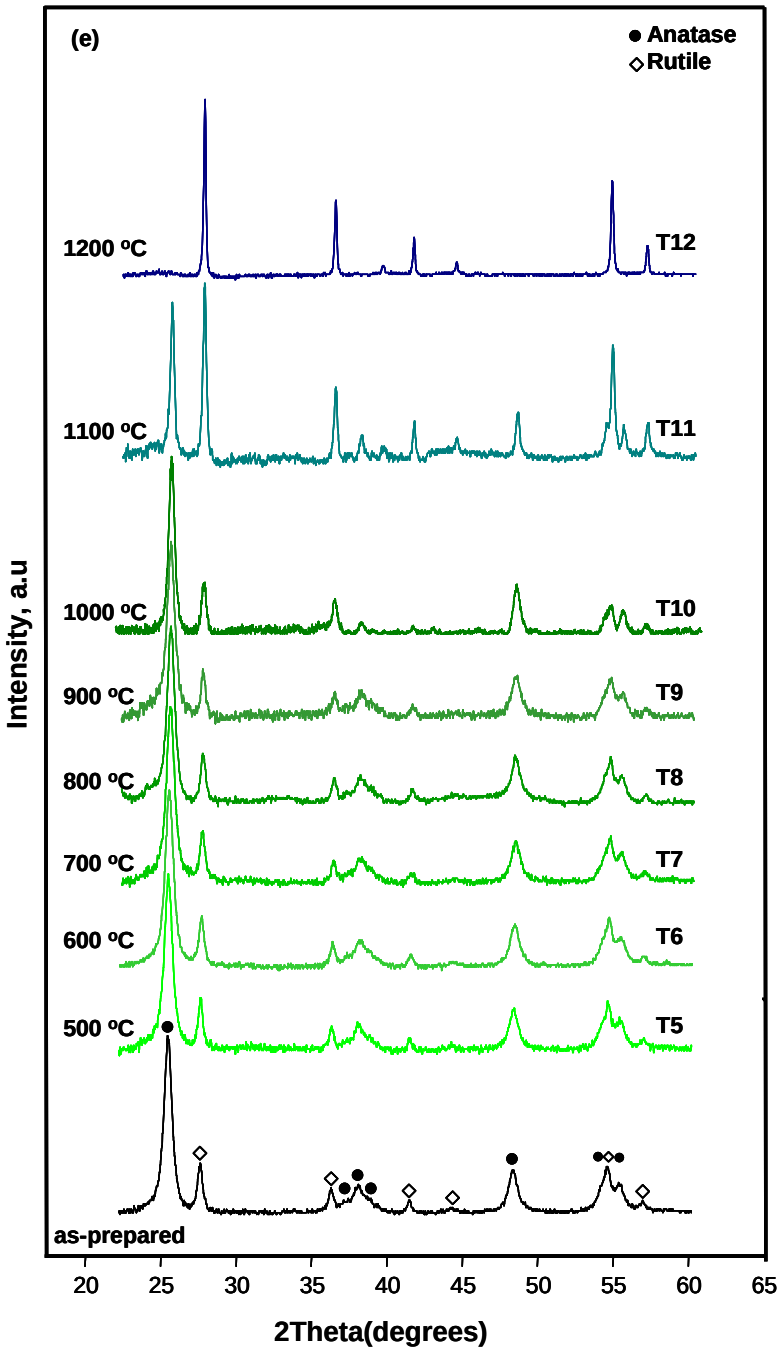

Figure A.e XRD patterns of TiO_2 with 24.84 % silica content, annealed under hydrothermal conditions.

APPENDIX B

XRD PATTERNS OF TiO_2/SiO_2 NANO-SIZED COMPOSITES CALCINED AT 500, 600, 700, 800, 900, 1000 and 1100 ^oC

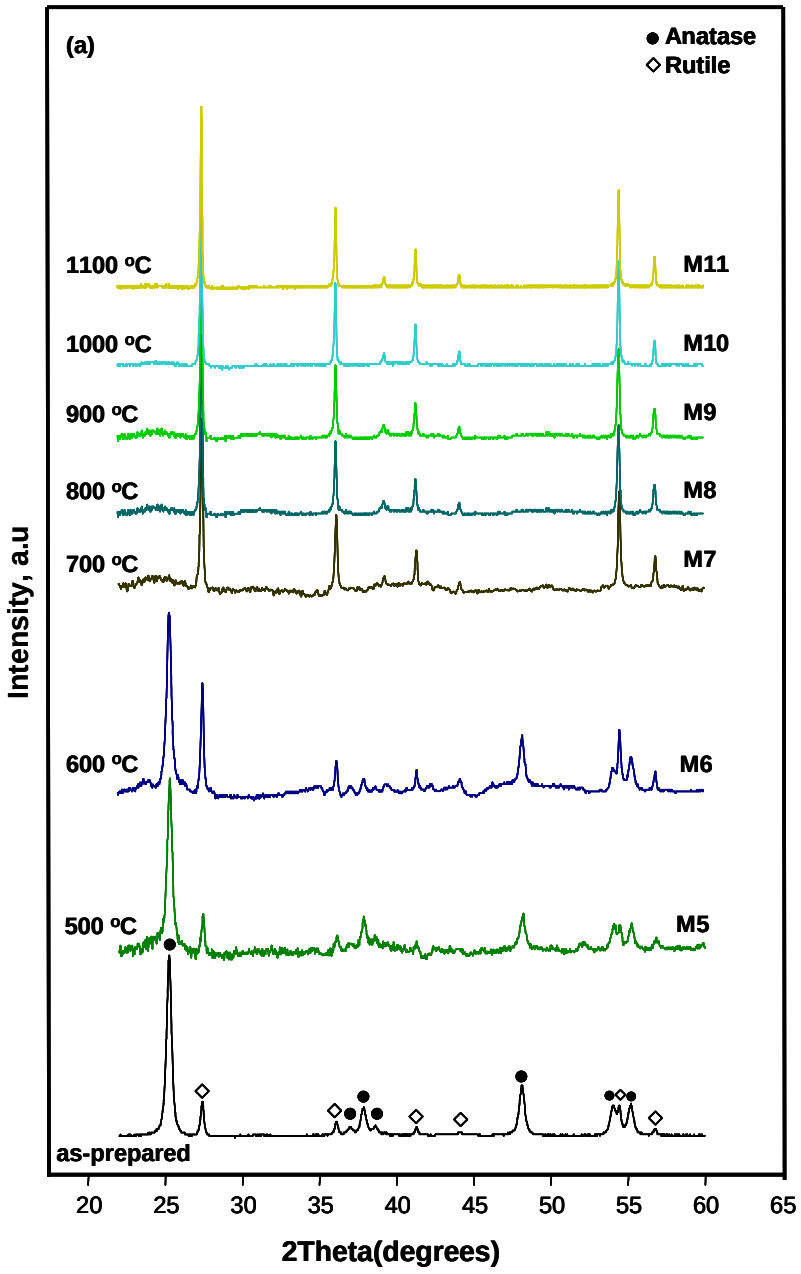

Figure B.a XRD patterns of TiO_2 with 0 % silica content, after thermal treatment.

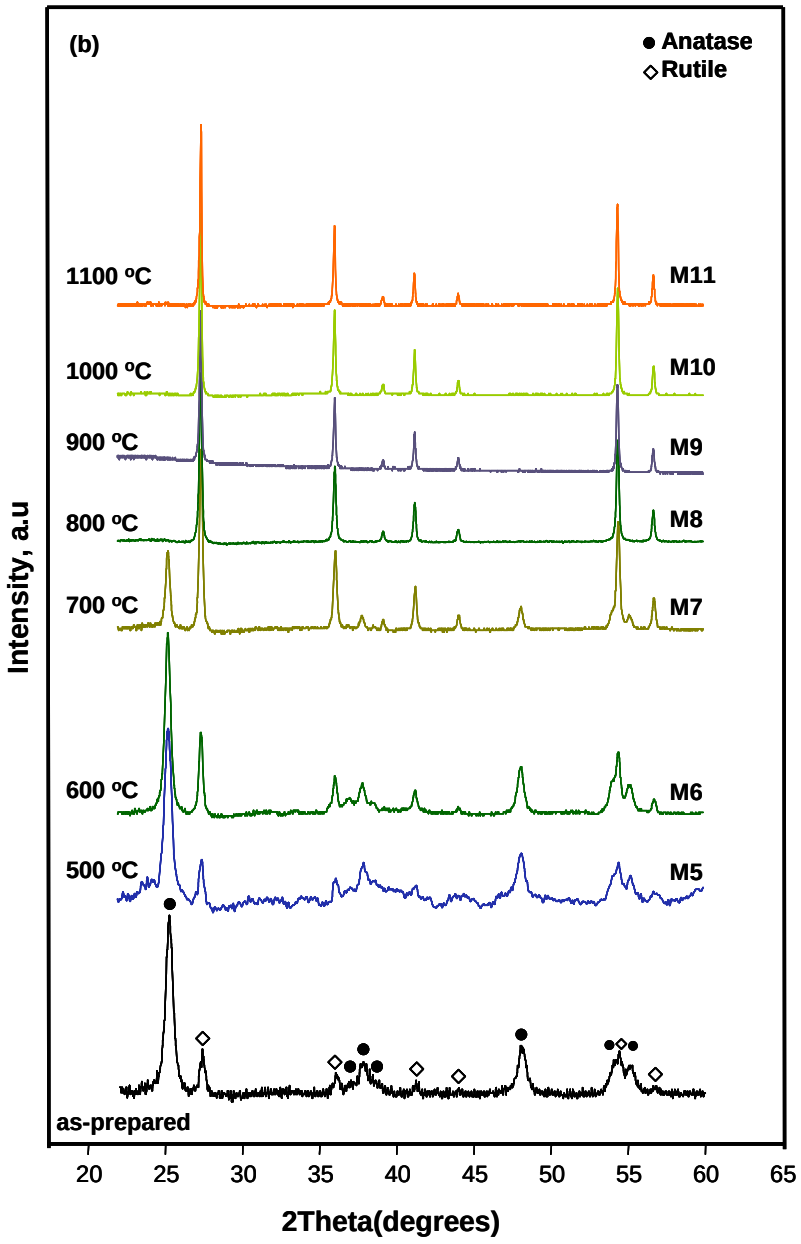

Figure B.b XRD patterns of TiO_2 with 0.54 % silica content, after thermal treatment.

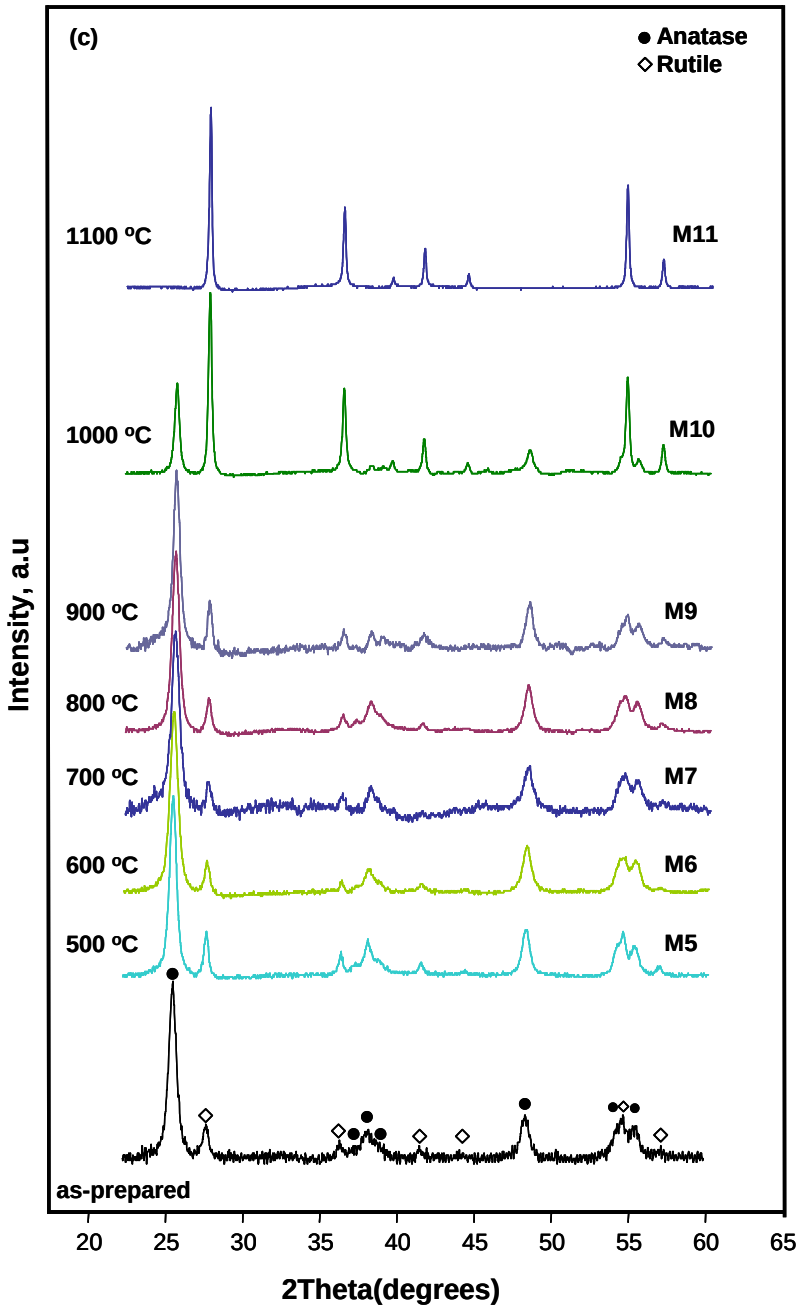

Figure B.c XRD patterns of TiO_2 with 4.53 % silica content, after thermal treatment.

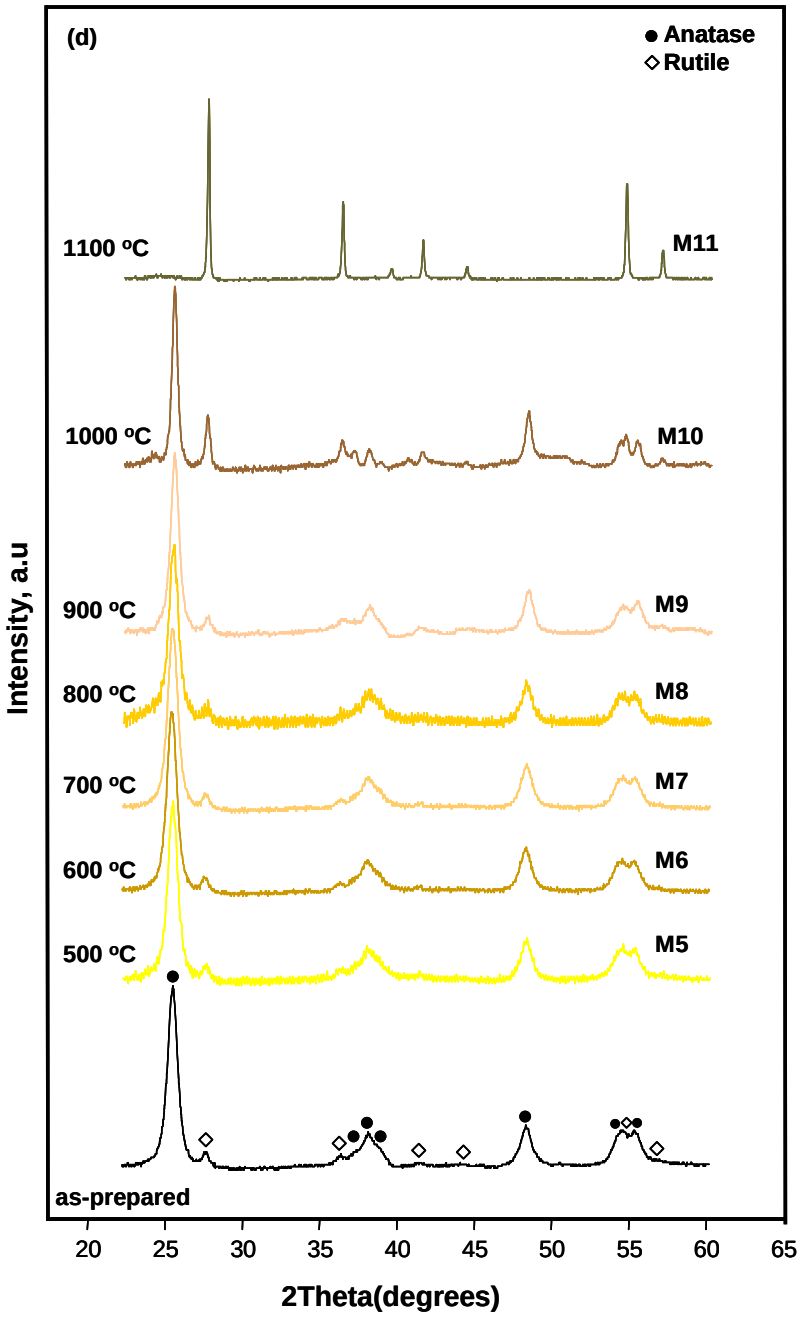

Figure B.d XRD patterns of TiO_2 with 9.71 % silica content, after thermal treatment.

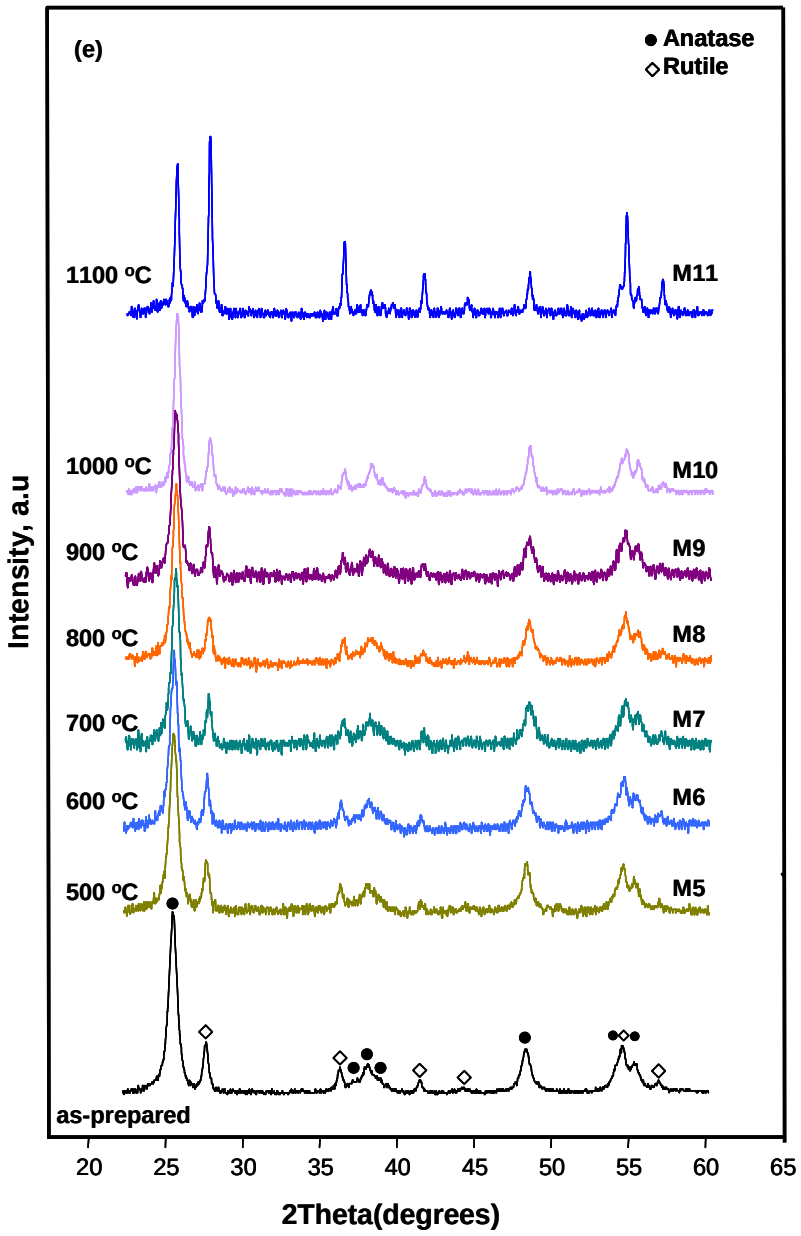

Figure B.e XRD patterns of TiO_2 with 24.84 % silica content, after thermal treatment.

BIBLIOGRAPHY

[1] B. Schimmoeller, H. Schulz, A. Ritter, A. Reitzmann, B. Kraushaar-Czarnetzki, A. Baiker, S. E. Pratsinis, *Journal of Catalysis* **2008**, 256, 74.

[2] M. A. L. Vargas, M. Casanova, A. Trovarelli, G. Busca, *Applied Catalysis B: Environmental* **2007**, 75, 303.

[3] K. Honda, A. Fujishima, *Nature* **1972**, 238, 37.

[4] G. Xu, Z. Zheng, Y. Wu, N. Feng, *Ceramics International* **2009**, *35,* 1-5.

[5] B. O'Regan, M. Grätzel, *Nature* **1991**, 353, 737.

[6] D. S. Burnside, K. Brooks, A. J. McEvoy, M. Grätzel, *Chimia* **1998**, 52 (10), 557.

[7] USP 5916947 (1999) Cape Cod Research.

[8] T. Saito, T. Iwase, J. Horie, T. J. Morioka, *Photochem. Photobiol. B* **1992**, 14, 369.

[9] EU-PS 218461 (1987) Raychem.

[10] L. Francioso, M. Prato and P. Siciliano, *Sensors and Actuators B: Chemical* **2008**, 128, 359.

[11] Y. Zhu, J. Shi, Z. Zhang, C. Zhang, X. Zhang, *Analytical Chemistry* **2002**, 74, 120.

[12] L. L. W. Chow, M. M. F. Yuen, P. C. H. Chan and A. T. Cheung, *Sensors and Actuators B:Chemical* **2001**, 76, 310.

[13] R. D. Shannon, J.A. Pask, J. *Am. Ceram. Soc.* **1965,** 48**,** 391.

[14] M. Hirano, K.Ota, H. Iwata, *Chem. Mater.* **2004**, 16 , 3725.

[15] G. Calleja, D. P. Serrano, R. Sanz, P. Pizarro, *Micropor. and Mesopor. Mater.* **2008**, 111, 429

[16] J. Ovenstone, K. Yanagisawa, *Chem. Mater.* **1999**, *11,* 2770.

[17] Q. Yang, C. Xie, Z. Xu, Z. Gap, Y. Du, *J. Phys. Chem. B* **2005**, 109, 5554.

[18] R. Jossen, M. C. Heine, S. E. Pratsinis, S. M. Augustine, M. K. Akhtar, *Applied Catalysis B: Environmental* **2007**, 69, 181.

[19] D. C. Hurum, A. G. Agrios, K. A. Gray, *J. Phys. Chem. B* **2003**, 107, 4545.

[20] H. Zhang, J. F. Banfield, *J. Mater. Chem.* **1998**, 8, 2073.

[21] Inorganic Crystal Structure Database (ICSD), **2009**, FIZ Karlsruhe: Germany.

[22] Diamond Demo-Version 3.2a, **2009**, K. Brandenburg.

[23] J. Lin, J. C. Yu, *J. Photochem. and Photobiol. A: Chemistry* **1998**, 116, 63.

[24] Y. R. Do, W. Lee, K. Dwight, A. Word, J. Solid State Chem. **1994**, 108, 198.

[25] P. Periyat, K. V. Baiju, P. Mukundan, P.K. Pillai, K. G. K. Warrier, *Applied Catalysis A: General* **2008**, 349, 13.

[26] C.P.Sibu, S.R.Kumar, P.Mukundan, K. G. K. Warrier, *Chem. Mate*r. **2002**, 14, 2876.

[27] DP 830786 (1952) Degussa.

[28] Technical Bulletin, Fine Particles, Number 11, Evonik Degussa GmbH.

[29] Y. Iida, S. Ozaki, *J. Am. Ceram. Soc.* **1961**, 44, 120.

[30] J. A. Gamboa, D.M. Pasquevich, *J. Am. Ceram. Soc.* **2005**, 75, 2934.

[31] X. Pan, X. Ma, J. Solid State Chem. **2004**, 177, 4098.

[32] Technical Bulletin, Fine Particles, Number 80, Evonik Degussa GmbH.

[33] EE32 Series Data logging and analysis PC software. **2008**, Engerwitzdorf, Austria.

[34] Stoe WINXPOW 1.2, **2000**, Stoe & Cie GmbH: Darmstadt

[35] Match!, Demo-Version 1.9, **2009**, K. Brandenburg.

[36] http://www.icdd.com/resources/tutorials/files/Quantitative%20Analysis%20RIR.ppt

[37] C. Anderson and A. J. Bard, *J. Phys. Chem B.* **1997**, 101, 2611.

[38] K.J.D. MacKenzie, Trans. J. Br. Ceram. Soc. **1975**, 74, 121.

[39] S. Andersson, B. Collen, U. Kuylenstierna, A. Magneli, *Acta. Chem. Scand.* **1957,** 11, 1641.

[40] Technical Bulletin, Pigments, Number 56, Evonik Degussa GmbH.

[41] G. Hyoung Lee, J. Min Zuo, J. *Am. Ceram. Soc.* **2003**, 87, 473.

[42] Y.Hu, H.-L. Tsai, C.-L Huang, *Material Sci. and Eng. A.* **2003**, 344, 209.

[43] W.D. Kingery, H.K. Bowen, D.R. Uhlmann, Introduction to Ceramics, 2nd edition, Wiley, New York.**1976**, 58.

VITA

Semih Afyon was born in Konya-Turkey, on 11.11.1982. He completed his high school education at Konya Meram Fen Lisesi in 2001. He got his Bachelor of Science degree in Chemistry, as the top ranking student, from Koc University-Istanbul, in 2006. In 2007, he started his master studies in Material Science and Engineering program at Koc University. His current research interests are synthesis and characterization of solid state and nano-materials, lithium ion batteries and renewable energy systems.